Quaternary Science Reviews 279 (2022) 107400

Contents lists available at ScienceDirect

Quaternary Science Reviews

journal homepage: www.elsevier.com/locate/quascirev

The Ticino-Toce glacier system (Swiss-Italian Alps) in the framework of the Alpine Last Glacial Maximum

Sarah Kamleitner [a, *], Susan Ivy-Ochs [a], Giovanni Monegato [b], Franco Gianotti [c], Naki Akçar [d], Christof Vockenhuber [a], Marcus Christl [a], Hans-Arno Synal [a]

[a] Laboratory of Ion Beam Physics, ETH Zurich, Otto-Stern-Weg 5, 8093, Zurich, Switzerland
[b] Institute of Geosciences and Earth Resources, National Research Council, Via Gradenigo 6, 35131, Padova, Italy
[c] Dipartimento di Scienze della Terra, Università di Torino, Via Valperga Caluso 35, 10125, Torino, Italy
[d] Institute of Geological Sciences, University of Bern, Baltzerstrasse 1-3, 3012, Bern, Switzerland

ARTICLE INFO

Article history:
Received 13 October 2021
Received in revised form
13 January 2022
Accepted 21 January 2022
Available online 14 February 2022

Handling Editor: C. O'Cofaigh

Keywords:
Quaternary/Pleistocene
Glaciation
European Alps
Cosmogenic nuclides
Geomorphology (glacial)
Surface exposure dating
Last Glacial Maximum
Ticino-Toce glacier

ABSTRACT

We present a new glacier chronology from one of the major end moraine systems of the Southern Alps. Timing and extent of the Last Glacial Maximum (LGM) advance of the Ticino-Toce glacier were reconstructed in detail based on landform relationships and surface exposure dating. ^{10}Be and ^{36}Cl ages from 41 erratic boulders constrain the last maximum of the Ticino-Toce glacier to have lasted from 25.0 ± 0.9 ka to 19.9 ± 0.7 ka. Over this period of ca. 5000 years the Ticino-Toce glacier underwent only minor oscillations, during which the glacier front remained close to its LGM maximum position. Underpinned by our detailed geomorphological reconstruction, the ages further demonstrate that the Verbano piedmont lobe was significantly larger (about 200 km^2) than shown on recent maps. A short-lived glacier readvance around 19.7 ± 1.1 ka terminated internal to the LGM maximum margins. Collapse of the Verbano lobe must have set in soon after and final withdrawal from the foreland occurred no later than 19 ka. The new Ticino-Toce chronology matches temporal constraints of major glacier systems emerging from adjacent Alpine accumulation areas. This points to in-phase glacier advances across the Western Alps, apart from the southwestern massifs for which a slightly earlier reaching of the Late Pleistocene maximum position of the Lyon lobe was shown recently. A two- potentially three-fold LGM advance structure with intervening retreat intervals, as reported for two major amphitheatres (Garda, Tagliamento) to the east is distinctly not supported by our data for the Ticino-Toce glacier. This contrast in glacier behaviour between the central and eastern Southern Alps is ascribed to shifting precipitation patterns after ca. 23–22 ka, away from southern to predominantly northwestern air flow and a greater independence of southerly moisture transport for the central Southern Alps.

1. Introduction

The preserved geomorphological record along the Alpine forelands documents multiple Quaternary glaciations reaching far beyond the mountain margins (Ehlers and Gibbard, 2004; Penck and Brückner, 1909). Major Pleistocene end moraine systems on the southern side of the Alps (Fig. 1) such as the Rivoli-Avigliana (Ivy-Ochs et al., 2018), Ivrea (Gianotti et al., 2008, 2015), Garda (Monegato et al., 2017; Ravazzi et al., 2014), or Tagliamento amphitheatres (Monegato et al., 2007) are characterized by closely spaced, stacked moraine ridges. Early surveys attempted to decipher the amphitheatres' evolution primarily on pedostratigraphical, morphostratigraphical and lithostratigraphical bases (Bini, 2012; Hantke, 1983; Penck and Brückner, 1909; Venzo, 1965). Differentiation, correlation and temporal relations of glaciogenic deposits and moraines represent critical uncertainties of this approach. The development of numerical chronological dating methods in the 20th century (e.g. radiocarbon dating, surface exposure dating, luminescence dating) and their applicability for a

* Corresponding author. Laboratory of Ion Beam Physics, ETH Zurich, Otto-Stern-Weg 5, HPK G26, 8093, Zurich, Switzerland.
E-mail addresses: kamsarah@phys.ethz.ch (S. Kamleitner), ivy@phys.ethz.ch (S. Ivy-Ochs), giovanni.monegato@igg.cnr.it (G. Monegato), franco.gianotti@unito.it (F. Gianotti), akcar@geo.unibe.ch (N. Akçar), vockenhuber@phys.ethz.ch (C. Vockenhuber), mchristl@phys.ethz.ch (M. Christl), synal@phys.ethz.ch (H.-A. Synal).

https://doi.org/10.1016/j.quascirev.2022.107400

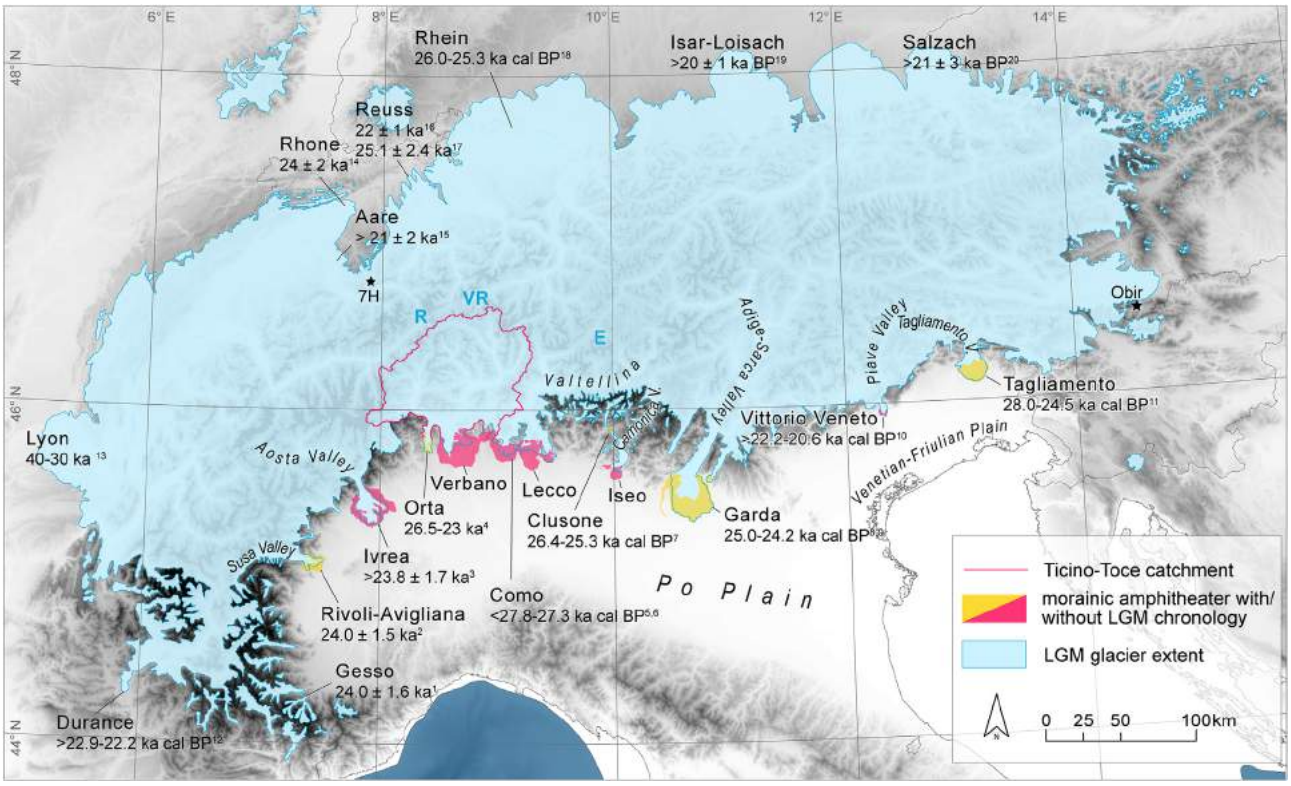

Fig. 1. Reconstructed extent (updated after Ehlers et al., 2011) and timing ((1) Federici et al., 2017; (2) Ivy-Ochs et al., 2018; (3) Gianotti et al., 2015; (4) Braakhekke et al., 2020; (5) Castelletti et al., 2013; (6) Bernoulli et al., 2018; (7) Ravazzi et al., 2012a; (8) Ravazzi et al., 2014; (9) Monegato et al., 2017; (10) Carton et al., 2009; (11) Monegato et al., 2007; (12) Jorda et al., 2000; (13) Gribenski et al., 2021; (14) Ivy-Ochs et al., 2004a; (15) Wüthrich et al., 2018; (16) Reber et al., 2014; (17) Gaar et al., 2019; (18) Preusser et al., 2007; (19) Reuther et al., 2011 (20) Starnberger et al., 2011) of Alpine glaciation at the LGM culmination. Locations of proposed LGM ice domes (Florineth and Schlüchter, 1998) are shown: R = Rhone ice dome, VR = Vorderrhein ice dome, E = Engadin ice dome. Stars indicate locations of Sieben Hengste (7H) and Obir cave systems (Luetscher et al., 2015; Spötl et al., 2021). Elevation data provided by GEBCO Compilation Group (2020).

suite of target materials, promised to overcome named limitations. Today glacial chronologies are mainly combined from radiocarbon dates in lacustrine (Larocque and Finsinger, 2008; Lister, 1988) and glacial sediments (Monegato et al., 2007, 2017; Ravazzi et al., 2012a), cosmogenic nuclide dating of former ice margins (Braakhekke et al., 2020; Federici et al., 2017; Gianotti et al., 2008, 2015; Ivy-Ochs et al., 2018), or OSL dating of glacial outwash (Gaar et al., 2019; Gribenski et al., 2021; Preusser et al., 2007). By use of modern dating techniques, recent studies were able to confirm that the majority of Italian Alpine and Swiss South-Alpine end moraine systems hold multiple ice-marginal complexes of LGM maximum age deposited by fluctuating glaciers between 28 and 23 ka (Bernoulli et al., 2018; Braakhekke et al., 2020; Ivy-Ochs et al., 2018; Monegato et al., 2007, 2017; Ravazzi et al., 2012a). Internal moraine ridges, could further be ascribed to late LGM readvance or recessional positions after 23 ka (Braakhekke et al., 2020; Carton et al., 2009; Gianotti et al., 2008, 2015; Ivy-Ochs et al., 2018; Monegato et al., 2007, 2017; Ravazzi et al., 2012a). Many of these stacked moraines had earlier been attributed to several pre-LGM glaciations (Balestro et al., 2009; Bini et al., 2014; Bini and Zuccoli, 2004; Carraro et al., 1975; Carraro and Petrucci, 1969; Feruglio, 1925, 1929; Petrucci, 1970; Sacco, 1892, 1927; Venzo, 1965).

As in other parts of the Alps, first studies on the Ticino-Toce glaciation around Lake Maggiore date back to the second half of the 19th and early 20th century (de Mortillet, 1861; Omboni, 1861; Penck and Brückner, 1909; Sacco, 1892; Taramelli, 1870). Over time, several interpretations for the size of the glacier of the Late Würm (*sensu* Chaline and Jerz, 1984; lately attributed to the LGM (Bini et al., 2009)) were proposed (Castiglioni, 1940; Hantke, 1983; Jäckli et al., 1970). Suggestions vary by up to 355 km^2 in extent of the piedmont lobe and 15 km in glacier length (Fig. 2a–d). Overall, Castiglioni (1940; Fig. 2c) claimed the largest Würm piedmont lobe while the most recent interpretation by Bini et al. (2009; Fig. 2a) is the most conservative LGM reconstruction. Based on relative soil formation and weathering depths, Penck and Brückner (1909; Fig. 2d) attributed large parts of the amphitheatre to Würm 'Jungmoränen' and categorized more external glacial deposits to a penultimate glaciation (in classical terms, Rissian 'Altmoränen'). In a later compilation based on Italian geological maps, Hantke (1983) suggested a similar Würm limit ('Äussere Jung-Endmoräne'; Fig. 2b) but discriminated and related outer glacial deposits to two pre-LGM glaciations (Riss and Mindel). In stark contrast to earlier interpretations based on the fourfold glaciation model (Günz, Mindel, Riss, and Würm) of Penck and Brückner, Bini (1997) recognized eleven different glaciogenic units building up the Verbano amphitheatre in addition to two more units underlying the end moraine system (Bini, 2012). Each was proposed to correlate to an independent glaciation (Bini, 1997). The last glacial episode is regionally referred to as the Cantù glaciation (Bini, 1997). In analogy to nine glaciations of proposed Middle Pleistocene age, the Cantù glaciation was distinguished on the basis of the thickness of the soil profile and weathered cortex of clasts (Bini and Zuccoli, 2004). The three oldest glaciations were dated to the early Pleistocene using U/Th dating, pollen analysis and/or paleomagnetic methods (Bini, 1997; Bini and Zuccoli, 2004; Uggeri et al., 1997). Numerical chronological data is scarce and only two radiocarbon ages were reported from the termination area of the Ticino-Toce paleoglacier. Both dates yield minimum ages for downwasting of the Verbano

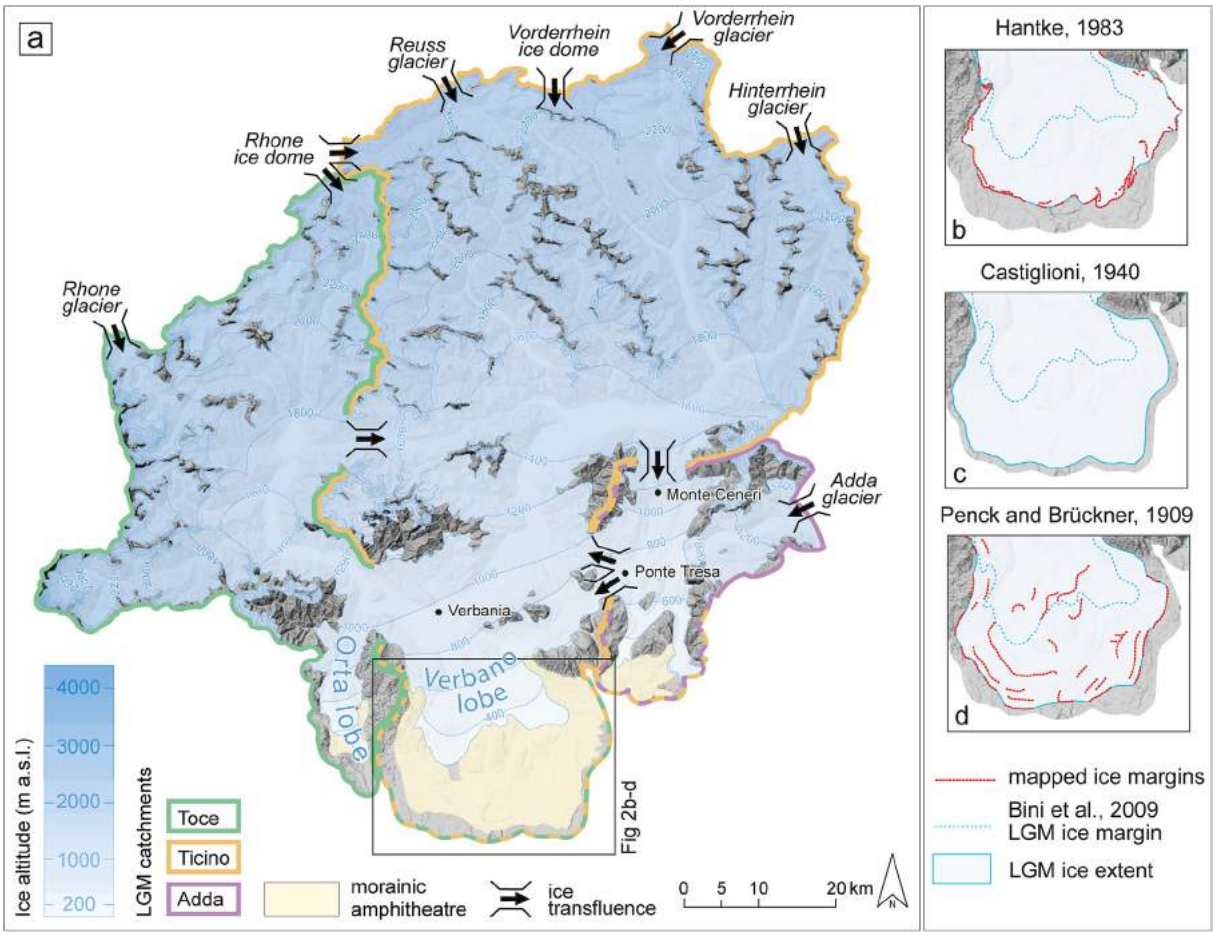

Fig. 2. Ticino-Toce paleoglacier system and major ice transfluences from and to neighbouring catchments during the last glaciation based on Bini et al. (2009; data provided by the Federal Office of Topography swisstopo). Inset maps (b–d) highlight selected suggestions on LGM extent of the Verbano lobe of Hantke (1983), Castiglioni (1940), and Penck and Brückner (1909) that have been georeferenced based on analogue maps. Elevation data provided by the European Union, Copernicus Land Monitoring Service 2020, European Environment Agency.

lobe (16.3–15.7 ka cal BP (Scapozza et al., 2014), 19.9–18.8 ka cal BP (Rey et al., 2020)).

Looking at the areas that have been studied in detail (Fig. 1), a distinct gap exists in the centre of the Southern Alps corresponding to the Ticino-Toce glacier system and Adda glacier system (flowing out from Valtellina). With their study of the Orta lobe, the smaller of two outlets of the Toce glacier, Braakhekke et al. (2020) took a first step towards the establishment of a regional glacier chronology for the central Southern Alps. The present study complements recent results by focusing on the whole Ticino-Toce glacier system and the associated Verbano amphitheatre. It provides a comprehensive reconstruction of one of the largest glacier networks of the Alps. Moreover, the central location of the Ticino-Toce catchment, its connection to the proposed Rhone- and Vorderrhein ice domes (Fig. 1; Fig.2a; Florineth and Schlüchter, 1998), and its linkages to other major glacier systems (Rhone glacier, Aare glacier, Reuss glacier, and Rhein glacier) provides insights on LGM processes beyond the watershed. Understanding the temporal evolution of the Ticino-Toce paleoglacier may therefore add crucial insights into (dis)similarity of Late Pleistocene glacier timing along as well as across the European Alps.

2. Study area

The Ticino-Toce catchment is situated in the Western Alps, south of the main Alpine divide. The roughly 6700 km^2 sized basin is located in Switzerland and Italy in equal parts. The northern sections of the study area belong to the Swiss cantons of Valais and Ticino. The southern parts of the catchment lie within the Italian regions of Piedmont and Lombardy (Fig. 3).

2.1. Geomorphological and geological setting

The drainage basin of the LGM Ticino-Toce system is characterized by its circular shape with a maximum N–S and E-W extension of about 100 km (Fig. 3). The dendritic valley network connects to two trunk valleys of Ticino River and Toce River leading down to the south. Elevation is unequally distributed across the catchment. Highest peaks are located to the west along the Monte Rosa-Fletschorn line (Fig. 3) with up to above 4600 m a.s.l. (above sea level). High-level accumulation areas in the eastern and northern parts are generally lower by about 1000 m.

In the southern parts of the study area, a number of lakes are encircled behind the Verbano end moraine system (Fig. 3). Lake Maggiore, which covers about 210 km^2 of the former Ticino glacier valley, is the largest one. While its width is often only a few kilometres, the lake length extends over more than 60 km filling the lower Ticino Valley floor. Present-day lake surface lies at 193 m a.s.l., but the water column reaches down to 179 m below sea level. Below the water column, two distinct sediment units of 100 m and 400 m thickness were inferred from seismic-reflection and refraction profiling (Finckh et al., 1984). Both are interpreted as of

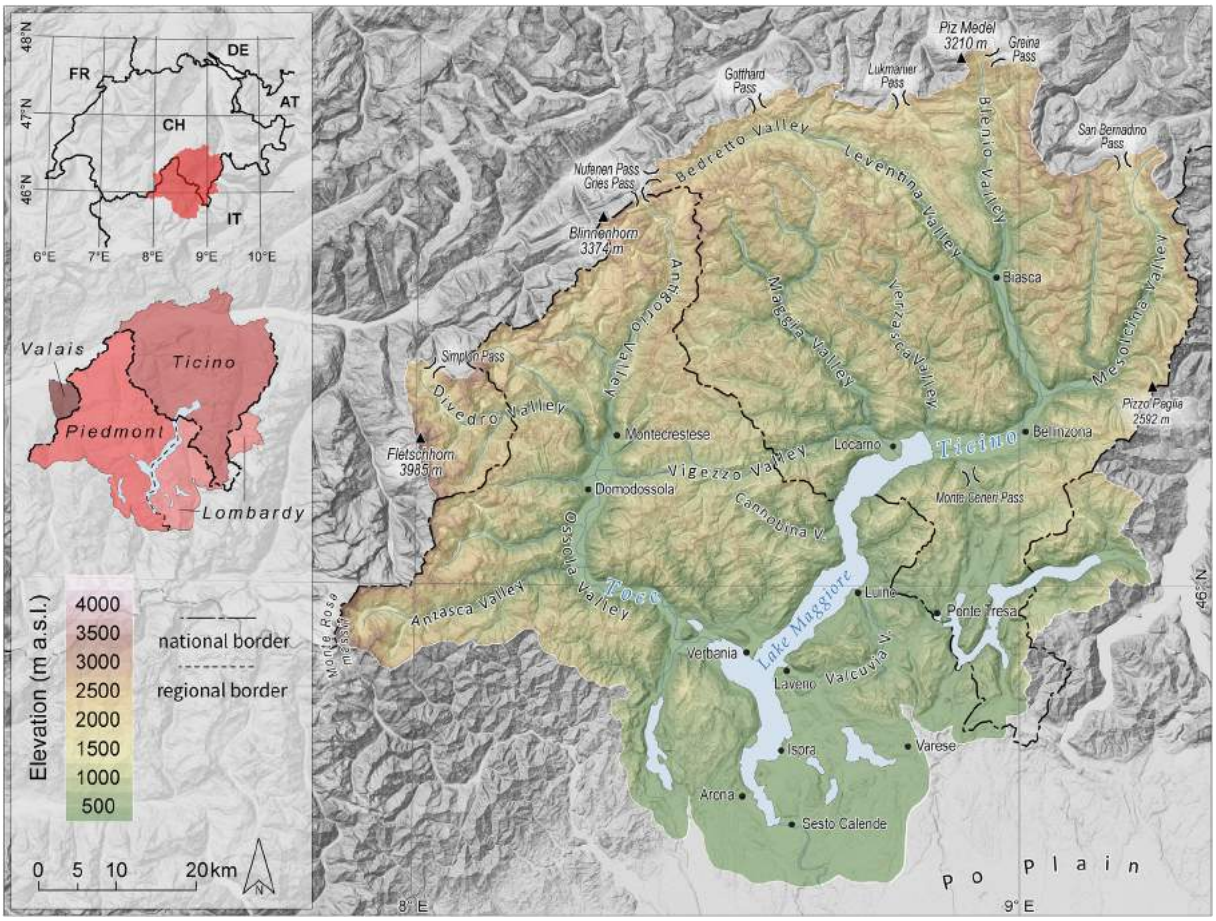

Fig. 3. Ticino-Toce watershed in the Swiss-Italian Alps. Elevation data provided by European Union, Copernicus Land Monitoring Service 2020, European Environment Agency.

glaciolacustrine origin (Finckh et al., 1984). A recent assessment of seismic data reveals a narrow trough upstream of Verbania (Fig. 3) characterized by basin and swell topography with depths well below sea level (Cazzini et al., 2020). Top of bedrock was reported at 600 m below sea level in the plain south of Bellinzona, progressively decreasing to maximum basin depth of 800 m below sea level half way between Luino and Laveno (Fig. 5; Cazzini et al., 2020). In the distal part of the valley, bedrock is generally shallower with a mean depth of 500 m below sea level (Cazzini et al., 2020). The deep basin of Lake Maggiore is, similar to other valleys in the south, assumed to have formed during the Messinian Salinity Crisis (Bini et al., 1978; Finckh, 1978). A drastic drop of Mediterranean Sea level triggered enhanced fluvial incision upstream and formation of Messinian canyons on the southern slopes of the Alps (Bini et al., 1978; Finckh, 1978; Preusser et al., 2010), that were filled by Messinian, Pliocene, Pleistocene and Holocene deposits as highlighted for the southern part of Switzerland (Bernoulli et al., 2018). In a recent study, Winterberg et al. (2020) showed that, in analogy to overdeepened basins on the northern side of the Alps, glacial erosion must also explain bedrock topography in inner Alpine valleys in the south.

The bedrock of the Toce-Ticino mountain basin can be split into two major domains (Dal Piaz, 2010): (a) the South Alpine domain with a Paleozoic basement lacking evidence of Alpine metamorphism and Mesozoic sedimentary covers; (b) the second domain grouping the Sesia Lanzo Zone and the Penninic and Helvetic nappes, characterized by a stack of basement and cover nappes with high-pressure Alpine metamorphism of Cretaceous age and a Tertiary greenschist to amphibolite facies overprinting (Lepontine Dome: Frey et al., 1999; Oberhänsli et al., 2004). The Periadriatic/Insubric line, a major tectonic feature of the Alps, separates the two domains and pinches the Canavese Zone slice to the west, while to the east the western tail of the Oligocene Bergell batholith (tonalite and granodiorite; Gianola et al., 2014) follows the lineament SE of Bellinzona. The northern tip of Lake Maggiore cross-cuts the Insubric line. Lake Maggiore is therefore situated in the western South Alpine domain dominated by Palaeozoic metamorphic rocks called Massiccio dei Laghi (Brack and Ulmer, 2010), which were intruded by Early Permian plutons (Federal Office of Topography swisstopo, 2005; Montrasio et al., 1990; Piana et al., 2017). The Massiccio dei Laghi is divided into the Ivrea-Verbano Zone and the Serie dei Laghi. The Permian, Meso-, and Cenozoic volcano-sedimentary cover of the Serie dei Laghi crops out near Arona and widens on the eastern side of Lake Maggiore from Laveno to the south (marine carbonate and clastic succession; Federal Office of Topography swisstopo, 2005; Montrasio et al., 1990; Piana et al., 2017).

2.2. Ticino-Toce glacier system

Ticino valley glacier emerged from inner Alpine accumulation areas along Bedretto Valley and was additionally fed by ice overflowing from the Rhone ice dome (Fig. 2a) to the east via Nufenen Pass (Fig. 3). With the existing ice divide on Gotthard Pass the ice supply of the Ticino glacier was additionally coupled to those of the Reuss glacier system (Fig. 1; Fig. 2a; Florineth and Schlüchter, 1998;

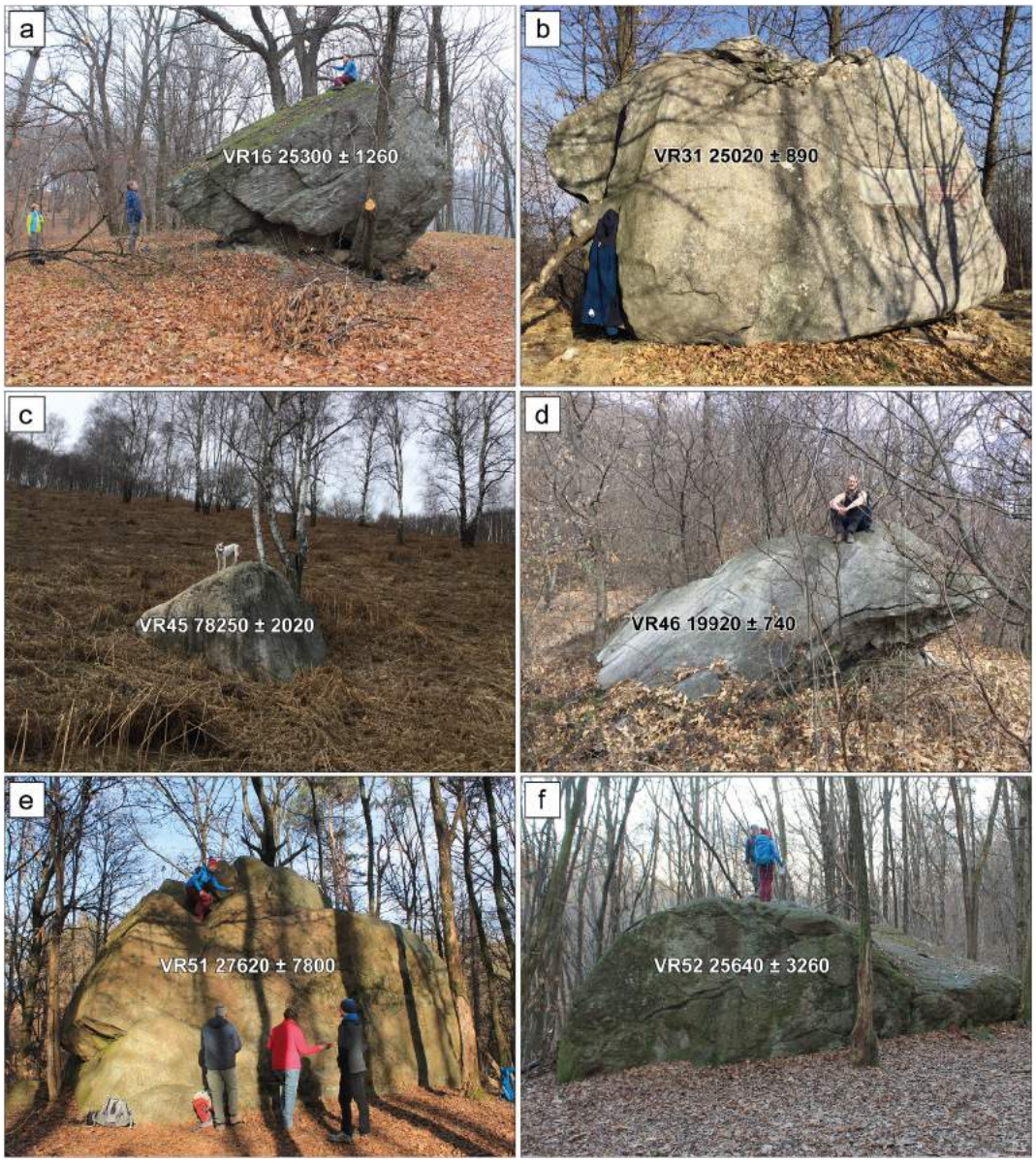

Fig. 4. Selected erratic boulders sampled in the Verbano amphitheatre and their surface exposure ages (a). Details on boulder characteristics can be found in Tables 1 and 2.

Hantke, 1983; Hippe et al., 2014). Downstream of Leventina Valley (Fig. 3), the Ticino glacier was joined by ice draining Blenio and Mesolcina valleys. Both tributaries were influenced by transfluences from Vorderrhein ice dome via Lukmanier and Greina passes and from Hinterrhein accumulation areas via San Bernardino Pass (Florineth and Schlüchter, 1998; Scapozza and Ambrosi, 2021), respectively (Fig. 2a; Fig. 3). Major contributions to the Ticino glacier were coming in from the right-hand side. These include ice from Verzasca and Maggia valleys, as well as Toce ice overflowing through Vigezzo and Cannobina valleys. An ice diffluence over Monte Ceneri Pass created a connection between the Ticino and Adda glacier systems. Parts of the ice masses from the Adda catchment re-entered the Ticino catchment at Valcuvia Valley through an overspill around Ponte Tresa (Fig. 2a). Advancing southwards, the large Ticino glacier filled the deep basin of Lake Maggiore and merged with Toce glacier coming in from the west around the city of Verbania.

In its upper sector, Toce catchment was dominated by ice draining through Divedro and Antigorio valleys (Fig. 3). Additionally, the Toce glacier received ice overflowing from the Rhone glacier via Simplon Pass and through a direct link to the Rhone ice dome at Gries Pass (Fig. 2a; Fig. 3; Florineth and Schlüchter, 1998; Kelly et al., 2004). In the centre of the Ossola Valley, ice of the Toce catchment did overflow into the Ticino catchment (Boriani and Burlini, 1995). At the mouth of the Anzasca Valley, Toce glacier coalesced with its major tributary glacier originating in the eastern slope of the Monte Rosa massif. Downstream from this confluence, the right side of the Toce glacier branched off to the south into the Orta basin, building up the correspondent Orta glacier lobe and Orta morainic amphitheatre (Fig. 2a; Braakhekke et al., 2020). The main branch of the Toce glacier continued eastward, overtopped the Mont'Orfano granite knob (794 m a.s.l.; Fig. 5), and merged with Ticino glacier.

Downstream of the confluence at Verbania, the merged Ticino-Toce glacier filled the southern parts of Lake Maggiore basin and advanced several kilometres towards the SSE. In the absence of

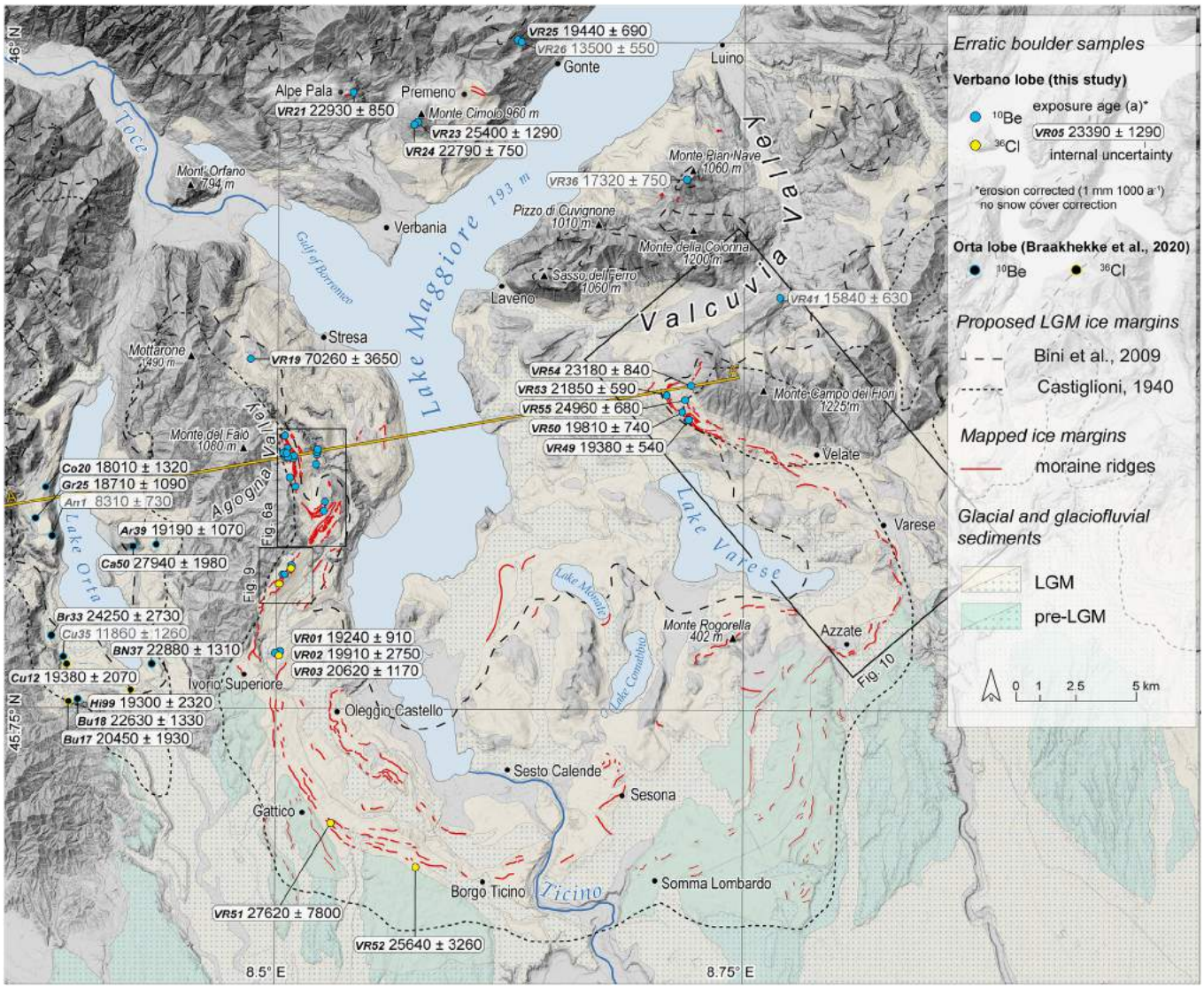

Fig. 5. Locations and surface exposure ages (a) of dated erratic boulders in the Verbano (this study) and Orta (Braakhekke et al., 2020) amphitheatres. Ages likely affected by post-depositional processes are shown in grey. LGM ice margin of Castiglioni (1940) was georeferenced on basis of an analogue map (see section 3.1). Moraine ridges were mapped on site and/or based on 5 m digital elevation models. Distribution of glaciofluvial and glacial sediments was adopted from the geological maps of Piedmont (1:250′000; Piana et al., 2017) and Lombardy (1:250′000; Montrasio et al., 1990). Fig. 12 displays the topography of the shown cross-section (A-A′). Elevation data provided by the regional governments of Piedmont and Lombardy.

topographic control, the Ticino-Toce glacier terminated onto the Po Plain as a wide piedmont lobe (Fig. 1; Fig. 2a), also referred to as Verbano lobe (derived from the Roman name of Lake Maggiore). Over multiple glaciations, a multi-ridged morainic amphitheatre with adjacent outwash plains (Bini et al., 2014; Montrasio et al., 1990; Piana et al., 2017) built-up. Within the end moraine system, bedrock is only cropping out along deeply incised valleys or plateau cliffs, e.g. the Permian rhyolite reliefs at Arona and the Eocene/Oligocene sedimentary units around Lake Comabbio and Lake Monate (Fig. 5; Bini, 1997; Bini et al., 2014; Montrasio et al., 1990).

3. Material and methods

3.1. Geomorphological analysis

3.1.1. Field surveys

Several field visits were carried out between November and March in the years from 2018 to 2021. Ice-marginal areas, earlier identified on the basis of digital elevation data, were traversed across the study area. During the survey, morphological characteristics and spatial relationships between landforms were recorded together with descriptions of surface material present. Wherever exposed (e.g. along road cuts, stream channels, excavation pits), lithostratigraphical and sedimentological information on glaciogenic deposits was included. Observations from the field build the basis for landform interpretation, complement, and 'ground truth' remote mapping results. Moraine ridges were further carefully searched for erratic boulders (>1 m high) in positions suitable for surface exposure dating (Ivy-Ochs and Kober, 2008).

3.1.2. Used geodata and landform analysis tools

Local observations from the field were complemented by geomorphological analysis on the basis of remotely sensed geodata, enabling larger scale landscape correlations. Elevation data, topographic and geologic maps were kindly provided by the Swiss

Federal Office of Topography swisstopo, the Italian National Geoportal Services, and the geodata portals of the Regional Offices of Piedmont and Lombardy. The latter provided 5 × 5 m digital elevation models on their regional territory. High resolution LiDAR data is additionally available area-wide for Switzerland (2–0.5 m resolution) and more spatially restricted to stream courses for the Italian parts of the catchment (1 m resolution). Supplied geodata of various spatial references were projected to a uniform geodetic coordinate reference system. The elevation models and their derivatives such as hillshade, slope and aspect models set the basis for landform analysis performed in a GIS environment. Noticeable variations in quality of provided elevation data led to differences in the level of geomorphological detail identified. This particularly concerns the Lombardian parts of the study area and could not always be compensated for with field visits. For intercomparison, early glaciation maps available in analogue form only, were georeferenced before digitization. Notably, this is the case for the reconstructions shown in Fig. 2b–d by Penck and Brückner (1909), Castiglioni (1940), and Hantke (1983). Achieved RMS errors lie between 25 m and 175 m. All GIS work was conducted using ESRI ArcMap 10.6 software equipped with ArcGIS Spatial Analyst extension. Post-processing was performed using Adobe Illustrator 2020 software.

3.2. Surface exposure dating

For surface exposure dating, erratic boulders were sampled with angle grinder, hammer, and chisel (Fig. 4). For each, boulder and sample details, boulder position, and shielding parameters were recorded (Table 1, Table 2). Sample preparation was performed at the Laboratory of Ion Beam Physics, ETH Zurich and at the Institute of Geological Sciences, University of Bern. Quartz bearing lithologies, used for ^{10}Be analysis, were crushed to grain size <800 μm using a hydraulic press. For non-quartz bearing samples processed for ^{36}Cl, a grain size range of 250–400 μm was used.

3.2.1. ^{10}Be exposure dating

Thirty-six rock samples successfully underwent selective chemical dissolution to isolate quartz (Kohl and Nishiizumi, 1992). Purified quartz was used for Be extraction procedure following Kronig et al. (2018, and references therein). ^{10}Be/^{9}Be ratios were determined with accelerated mass spectrometry (AMS) using the 0.5 MV TANDY and 0.3 MV MILEA systems at the Laboratory of Ion Beam Physics, ETH Zurich and normalized to the in-house ^{10}Be standard S2007N with nominal ratio of 28.1 × 10^{-12} (calibrated to 07KNSTD; Christl et al., 2013). AMS set-up and normalization of Be data are described in detail in Christl et al. (2013). Measured Be ratios were corrected with a running mean and full process blank of 2.7–3.8 × 10^{-15} (Table 1). ^{10}Be exposure ages were calculated with the CRONUS-Earth online calculator (Balco et al., 2008) using the Northeastern North American (NENA, version 2.2) calibration data set (Balco et al., 2009) and the scaling scheme of Lal (1991) and Stone (2000). Claude et al. (2014) have recently demonstrated the suitability of NENA production rates for the Alps. Internal and external uncertainties are reported as 1σ errors. Both include uncertainties associated with AMS measurement and blank correction. External errors additionally account for uncertainties in nuclide production rates (Balco et al., 2008). Rock density of 2.7 g cm^{-3} was used. Surface weathering was accounted for with an erosion rate of 1 mm ka^{-1} (André, 2002). The applied erosion correction increased all except four exposure ages by less than 2.1%. For the four oldest boulders (VR19, VR30, VR42, VR45) the erosion correction is 6–8%. For the majority of the samples, the erosion-corrected age resides well within the associated internal age uncertainties. Solely for ages beyond 70 ka, does the erosion-corrected age exceed the associated internal uncertainties, and this is by 0.7–5.6%. Ages were not corrected for snow cover due to lack of reliable data on snow height and snow cover duration over the past millennia. A 78-year monthly snow record from above Locarno (367 m a.s.l.) yields a mean snow cover of 2 cm for three months per year for the mid-20th to early-21st century (Federal Office of Meteorology and Climatology MeteoSwiss, 2016). This correction would increase calculated ages by 0.1% (median and mean value). Erosion-corrected ^{10}Be exposure ages range from 12.7 ± 1.1 ka to 101.9 ± 2.7 ka (Table 1)

3.2.2. ^{36}Cl exposure dating

Five samples from non-quartz bearing lithologies (unsuitable for ^{10}Be dating) were prepared for cosmogenic ^{36}Cl exposure dating. Whole-rock sample preparation is described in detail in Stone et al. (1996), Ivy-Ochs (1996), and Ivy-Ochs et al. (2004b). AMS measurements were performed at the 6 MV TANDEM system at the Laboratory of Ion Beam Physics, ETH Zurich against K382/4N standard (^{36}Cl/Cl^{e} ratio of 17.36 × 10^{-12} calibrated against the primary ^{36}Cl standard KNSTD5000; Christl et al., 2013; Synal et al., 1997; Vockenhuber et al., 2019). Sample ratios were corrected for laboratory process blanks of 1.0 × 10^{-15}, 1.9 × 10^{-15}, and 3.3 × 10^{-15} (Table 2). Elemental compositions of leached aliquot samples were determined with ICP-MS by Actlabs (Ontario, Canada) and are reported in Table 3. ^{36}Cl exposure ages were calculated using an in-house MATLAB code based on constants and equations presented by Alfimov and Ivy-Ochs (2009). High latitude, sea level spallation production rates of 48.8 ± 3.4 at $g_{Ca}^{-1}a^{-1}$ (Stone et al., 1996), 162 ± 24 at $g_{K}^{-1}a^{-1}$ (Evans et al., 1997), 13 ± 3 at $g_{Ti}^{-1}a^{-1}$ (Fink et al., 2000), and 1.9 ± 0.2 at $g_{Fe}^{-1}a^{-1}$ (Stone et al., 2005) were used. Scaling scheme of Stone (2000) was applied. ^{36}Cl produced through muon interactions amounts to 9% and 6% from Ca and K, respectively (Evans et al., 1997; Stone et al., 1996, 1998). ^{36}Cl production via (epi) thermal neutron capture on ^{35}Cl is calculated using a neutron flux value of 760 $g_{air}^{-1}a^{-1}$ following Alfimov and Ivy-Ochs (2009, and references therein). Rock density of 2.7 g cm^{-3} was used. Applied parameters account for site as well as rock specific ^{36}Cl production rates and show good agreement with recently reported values (Borchers et al., 2016; Marrero et al., 2016). Natural Cl in four out of the five samples dated with ^{36}Cl was extremely low (7–19 ppm). In one sample (VR06) it was 312 ppm.

In analogy to ^{10}Be samples, ^{36}Cl exposure ages were corrected for surface weathering (1 mm ka^{-1}; André, 2002). Erosion correction lowers calculated ages by 5–9% (Table 2) and compares to internal and external age uncertainties of 12–28% and 14–29%, respectively. Snow correction was not applied due to insufficient knowledge on past snow patterns. Obtained ^{36}Cl exposure ages cover a time range of 15.8 ± 1.9 ka to 27.6 ± 7.8 ka (Table 2). Where both ^{10}Be and ^{36}Cl dating was performed on the same landform, exposure ages agree well with each other (hill top east of Invorio Superiore (VR01, VR02, VR03); inner moraine ridge between Fosseno and Colazza (VR06, VR07)).

In the aftermath of boulder deposition, various processes (e.g. exhumation, toppling, turning, or quarrying) may lead to a distortion of the gained exposure age towards the younger (Ivy-Ochs and Kober, 2008). While pre-exposure of erratic boulders is less often an issue, post-depositional processes commonly cause data scatter (Briner et al., 2005; Heyman et al., 2011; Ivy-Ochs and Kober, 2008; Putkonen and Swanson, 2003). We acknowledge that erratic surface exposure ages represent minimum ages for formation of the dated ice margin or deglaciation of the specific site, respectively. On account of incomplete exposure, we generally assess the oldest exposure age as preferential age of moraine deposition and do not calculate mean ages. In any case, the preferred age is often derived from the tallest boulder (Heyman et al., 2016) in the most stable

Table 1
Site information, sample details, and results of ^{10}Be exposure dated erratic boulders.

Sample ID	Location	Topographic position	Boulder lithology	Bouldersize L × W × H (m)	Latitude (°N)	Longitude (°E)	Elevation (m a.s.l.)	Sample thickness (cm)	Topographic shielding factor	^{10}Be concentration (10^5 at g^{-1})	Exposure age* 1 mm ka^{-1}erosion (ka)
				Western sector							
VR25[x]	Gonte	slope	gneiss	3.5 × 3.5 × 2.0	46.0005	8.6277	1015	2.0	0.985	1.761 ± 0.061[b]	19.4 ± 0.7 (1.2)
VR26[x]	Gonte	slope	gneiss	2.0 × 1.2 × 1.6	46.0002	8.6283	982	2.0	0.973	1.184 ± 0.047[b]	13.5 ± 0.5 (0.9)
VR21[x]	Alpe Pala	moraine crest	gneiss	1.9 × 1.2 × 1.6	45.9803	8.5383	896	2.5	0.991	1.881 ± 0.068[b]	22.9 ± 0.8 (1.4)
VR23[x]	Monte Cimolo	hill top	gneiss	1.5 × 2.0 × 1.2	45.9705	8.5740	963	1.5	1.000	2.232 ± 0.110[b]	25.4 ± 1.3 (1.8)
VR24[x]	Monte Cimolo	hill top	gneiss	1.9 × 2.0 × 1.0	45.9704	8.5739	962	3.5	1.000	1.973 ± 0.063[b]	22.8 ± 0.7 (1.3)
VR19[x]	Mottarone-Stresa	slope	granite	3.0 × 1.0 × 0.8	45.8805	8.4861	881	2.5	0.998	5.449 ± 0.262[c]	70.3 ± 3.6 (5.2)
VR42[y]	Alpe Canà, external	slope	granite	1.6 × 1.4 × 1.4	45.8453	8.5040	792	2.75	0.999	5.369 ± 0.104[f]	74.9 ± 1.6 (4.2)
VR28[x]	Alpe Canà, ridge 1	moraine crest	granite	2.0 × 2.0 × 1.5	45.8455	8.5048	805	2.0	1.000	1.831 ± 0.055[d]	**23.8 ± 0.7 (1.4)**
VR29[x]	Alpe Canà, ridge 1	moraine crest	granite	3.5 × 2.5 × 1.9	45.8448	8.5049	805	2.0	1.000	1.806 ± 0.057[f]	23.5 ± 0.8 (1.4)
VR30[x]	Alpe Canà, ridge 1-2	slope	granite	4.0 × 5.0 × 2.5	45.8437	8.5049	783	2.0	0.997	7.079 ± 0.169[c]	101.9 ± 2.7 (6.1)
VR44[y]	Alpe Canà, ridge 2	moraine slope	granite	3.0 × 1.0 × 1.3	45.8452	8.5058	797	1.5	0.999	2.291 ± 0.066[f]	30.1 ± 0.9 (1.7)
VR45[y]	S of Alpe Canà	slope	granite	6.0 × 4.0 × 4.0	45.8361	8.5077	795	1.0	0.988	5.623 ± 0.133[f]	78.3 ± 2.0 (4.6)
VR27[x]	Alpe Canà, ridge 3	moraine crest	gneiss	1.8 × 1.2 × 1.0	45.8470	8.5060	809	1.5	0.999	1.557 ± 0.081[c]	20.0 ± 1.1 (1.4)
VR43[y]	Alpe Canà, ridge 3	moraine crest	granite	2.0 × 1.5 × 1.2	45.8437	8.5065	764	1.25	0.999	1.643 ± 0.056[f]	**21.9 ± 0.8 (1.3)**
VR12[x]	Alpe Canà, ridge 5	moraine crest	mica schist[+]	3.0 × 2.0 × 0.8	45.8432	8.5093	757	1.75	0.993	1.273 ± 0.058[a]	17.2 ± 0.8 (1.2)
VR13[x]	Alpe Canà, ridge 5b	moraine crest	mica schist	5.0 × 2.0 × 1.4	45.8433	8.5094	757	2.0	0.998	1.451 ± 0.058[a]	19.6 ± 0.9 (1.3)
VR14[x]	Alpe Canà, ridge 5b	moraine crest	granite	1.6 × 1.0 × 1.0	45.8518	8.5048	818	2.25	1.000	1.416 ± 0.103[c]	18.1 ± 1.4 (1.6)
VR46[y]	S of Alpe Canà, ridge 5a	moraine crest	gneiss	8.0 × 3.0 × 3.0	45.8326	8.5105	746	1.5	0.990	1.458 ± 0.053[e]	**19.9 ± 0.7 (1.2)**
VR09[x]	Alpe della Cascine	moraine crest	gneiss	1.5 × 1.0 × 1.0	45.8271	8.5264	680	2.75	0.990	0.878 ± 0.061[a]	12.7 ± 0.9 (1.1)
VR10[x]	Alpe della Cascine	moraine crest	gneiss	1.8 × 1.5 × 0.6	45.8237	8.5257	646	2.5	0.999	0.865 ± 0.046[b]	12.7 ± 0.7 (0.9)
VR15[x]	Brovello	moraine crest	gneiss	10.0 × 4.0 × 2.5	45.8447	8.5219	569	1.75	0.977	1.206 ± 0.074[b]	19.4 ± 1.2 (1.5)
VR16[x]	Brovello	moraine crest	gneiss	7.0 × 3.5 × 5.0	45.8448	8.5220	571	2.0	0.999	1.599 ± 0.078[b]	25.3 ± 1.3 (1.8)
VR17[x]	Brovello	moraine crest	gneiss	2.5 × 1.7 × 1.2	45.8452	8.5222	573	3.0	0.987	1.149 ± 0.069[a]	18.4 ± 1.1 (1.4)
VR18[x]	Brovello	moraine crest	gneiss	2.0 × 2.0 × 1.8	45.8411	8.5216	558	3.8	0.971	1.187 ± 0.065[a]	**19.7 ± 1.1 (1.5)**
VR05[x]	Fosseno-Colazza, outermost ridge	moraine crest	gneiss	2.0 × 1.0 × 1.2	45.7998	8.5039	683	1.5	1.000	1.628 ± 0.088[a]	23.3 ± 1.3 (1.7)
VR31[y]	Fosseno-Colazza, outermost ridge	moraine crest	gneiss	3.0 × 2.2 × 3.5	45.7999	8.5051	674	2.0	1.000	1.725 ± 0.060[d]	**25.0 ± 0.9 (1.5)**
VR07[x]	Fosseno-Colazza, internal ridge	moraine crest	gneiss	1.7 × 1.7 × 1.3	45.8032	8.5086	633	2.75	0.993	1.221 ± 0.067[d]	18.4 ± 1.0 (1.4)
VR01[x]	E of Invorio Superiore	hill top	mica schist[+]	5.0 × 2.0 × 1.0	45.7710	8.5029	489	4.5	1.000	1.118 ± 0.052[a]	19.2 ± 0.9 (1.3)
VR03[x]	E of Invorio Superiore	hill top	gneiss	1.0 × 1.0 × 1.0	45.7704	8.5002	462	2.25	0.999	1.189 ± 0.066[a]	**20.6 ± 1.2 (1.5)**
				Eastern sector							
VR36[y]	Monte Pian Nave	slope	granite	2.5 × 2.5 × 1.2	45.9490	8.7203	1038	2.0	0.998	1.620 ± 0.068[f]	17.3 ± 0.7 (1.1)
VR41[y]	Valcuvia Valley	bedrock ridge	gneiss	1.0 × 1.9 × 1.5	45.9041	8.7698	530	2.5	0.992	0.965 ± 0.038[e]	15.8 ± 0.6 (1.0)
VR49[y]	Campo dei Fiori, lower ice margin	moraine crest	gneiss[+]	1.7 × 1.5 × 1.1	45.8583	8.7212	620	1.5	0.990	1.279 ± 0.035[f]	19.4 ± 0.5 (1.1)
VR50[y]	Campo dei Fiori, lower ice margin	moraine crest	gneiss	2.5 × 2.0 × 1.6	45.8613	8.7175	623	2.0	0.999	1.315 ± 0.048[e]	**19.8 ± 0.7 (1.2)**
VR53[z]	Campo dei Fiori, lower ice margin	moraine crest	gneiss[+]	5.0 × 3.0 × 1.5	45.8687	8.7092	650	3.75	0.990	1.447 ± 0.038[g]	21.8 ± 0.6 (1.2)
VR54[z]	Campo dei Fiori, higher ice margin	moraine crest	gneiss	2.6 × 1.5 × 1.2	45.8719	8.7217	791	1.5	0.998	1.770 ± 0.063[g]	23.2 ± 0.8 (1.4)
VR55[z]	Campo dei Fiori, higher ice margin	moraine crest	quartzite	2.5 × 1.5 × 1.3	45.8662	8.7196	694	2.5	0.987	1.721 ± 0.045[g]	**25.0 ± 0.7 (1.4)**

+ quartz vein sampled.
* external uncertainties in brackets.
[a,b,c,d,e,f,g] applied blank correction ratios of (a) 3.0 × 10^{-15}b) 3.1 × 10^{-15}(b) 3.1 × 10^{-15}, (c) 3.8 × 10^{-15}, (d) 3.3 × 10^{-15}, (e) 3.7 × 10^{-15}, (f) 3.3 × 10^{-15}, (g) 2.7 × 10^{-15}.
[x,y,z] sampled in (x) 2018, (y) 2020, (z) 2021.

position. The basic principle is applied unless contradictory geomorphological evidence and multiple other chronological data exist (e.g. in case of sample VR16).

Previously published surface exposure ages have been recalculated according to procedure and parameters described above. Erosion correction and snow shielding were treated as in original. All ^{14}C ages referenced have been calibrated using the OxCal 4.4 online calculator (Bronk Ramsey, 2009) and the IntCal20 calibration curve (Reimer et al., 2020) with 95.4% probability range.

4. Results: geomorphology and exposure dating

Remotely sensed data combined with field-based observations were used to map glacial landforms within the Verbano amphitheatre. ^{10}Be and ^{36}Cl surface exposure dating of suitable erratic boulders provides chronological evidence on the timing of deposition of the respective ice margin. The geomorphology of the study area and obtained exposure ages are outlined in detail in this section. Results are geographically grouped into three principle areas: (a) the nearly continuous right lateral moraine series in the west,

Table 2
Site information, sample details, and results of ^{36}Cl exposure dated erratic boulders.

Sample ID	Location	Topographic position	Boulder lithology	Boulder size L × W × H (m)	Latitude (°N)	Longitude (°E)	Elevation (m a.s.l.)	Sample thickness (cm)	Topographic shielding factor	^{36}Cl concentration (10^5 at g^{-1}_{rock})	Exposureage* no erosion (ka)	Exposureage* 1 mm ka^{-1} erosion (ka)
					Western sector							
VR06[x]	Fosseno-Colazza internal ridge	moraine crest	gabbro	6.0 × 3.0 × 3.0	45.8021	8.5084	643	3.0	1.000	4.703 ± 0.563[a]	16.6 ± 2.0 (2.8)	15.8 ± 1.9 (2.7)
VR33[y]	Fosseno-Colazza internal ridge	moraine crest	serpentinite	1.9 × 1.6 × 1.5	45.7963	8.5021	612	5.0	0.995	0.364 ± 0.062[b]	27.9 ± 4.7 (5.9)	25.5 ± 4.3 (5.5)
VR02[x]	E of Invorio Superiore	hill top	talcschist	5.0 × 4.0 × 2.0	45.7694	8.5023	478	1.5	1.000	0.703 ± 0.097[a]	20.9 ± 2.9 (3.1)	19.9 ± 2.7 (3.1)
					Frontal sector							
VR51[z]	SE of Gattico	moraine crest	serpentinite	8.0 × 3.0 × 6.0	45.7069	8.5311	336	2.0	0.987	0.352 ± 0.099[c]	29.4 ± 8.3 (8.5)	27.6 ± 7.8 (8.1)
VR52[z]	NW of Borgo Ticino	proglacial terrace	serpentinite	13.0 × 10.0 × 4.0	45.6907	8.5763	326	1.0	1.000	0.629 ± 0.080[c]	27.2 ± 3.5 (3.8)	25.6 ± 3.3 (3.7)

* external uncertainties in brackets.
[a,b,c] applied blank correction ratios of (a) 1.0×10^{-15}, (b) 1.9×10^{-15}, (c) 3.3×10^{-15}.
[x,y,z] sampled in (x) 2018, (y) 2020, (z) 2021.

Table 3
Elemental data for ^{36}Cl samples.

Sample ID	Al_2O_3 (wt%)	CaO (wt%)	Fe_2O_3 (wt%)	K_2O (wt%)	MgO (wt%)	MnO (wt%)	Na_2O (wt%)	P_2O_5 (wt%)	SiO_2 (wt%)	TiO_2 (wt%)	LOI (wt%)	Gd (ppm)	Sm (ppm)	Th (ppm)	U (ppm)	Cl* (ppm)
VR06	20.93	11.20	10.29	0.05	8.62	0.139	0.90	0.04	47.58	0.611	0.21	1.50	1.3	<0.1	<0.1	312.45 ± 7.38
VR33	1.90	0.12	12.15	<0.01	38.28	0.112	0.01	0.02	37.73	0.029	9.76	<0.10	<0.1	0.1	<0.1	11.80 ± 0.19
VR02	4.02	3.64	7.77	0.03	34.54	0.108	0.10	0.04	42.09	0.133	7.56	0.40	0.3	<0.1	<0.1	18.47 ± 0.41
VR51	1.70	1.34	7.96	<0.01	40.28	0.104	0.03	0.01	41.54	0.019	6.99	<0.10	<0.1	<0.1	<0.1	7.18 ± 0.15
VR52	3.97	2.91	7.67	<0.01	35.37	0.101	0.07	0.02	41.75	0.088	8.13	0.30	0.2	<0.1	<0.1	14.39 ± 0.30

* determined with AMS.

(b) the left lateral ice margins on the eastern side of the piedmont glacier and (c) the dissected frontal moraines at the former glacier terminus to the south (Fig. 5). Bold ages in Table 1 are considered most representative for time of landform deposition and are usually equivalent to the oldest exposure age available for the respective landform (cf. Heyman et al., 2011).

4.1. Western sector

The glacial imprint of Ticino-Toce glacier shows excellent preservation along the western part of the end moraine system. The number and extent of preserved glacial landforms thereby increases from patchy glacial deposits north of the Gulf of Borromeo (local sites of Gonte, Alpe Pala, Premeno and Monte Cimolo; Fig. 5) to multiple, nearly continuous lateral moraine sets at and below Alpe Canà, around Alpe della Cascine and above Brovello (Fig. 6a). Further to the south, the transition to the frontal sector of the piedmont lobe is recorded between the towns of Fosseno, Colazza, and Invorio Superiore (Fig. 5; Fig. 9).

Erratic boulders and patchy glacial sediments as evidence of former ice margins cover the shallow and steep bedrock slopes north of the Gulf of Borromeo (Fig. 5). Above the town of Gonte, glacial deposits were found up until 1050 m a.s.l. Boulder VR25 at an altitude of 1015 m a.s.l. gave an age of 19.4 ± 0.7 ka. This age likely represents a minimum age, as the boulder is located on a steep slope. The age of an adjacent boulder (VR26; 13.5 ± 0.5 ka) is considerably younger probably due to gravitational processes or burial. Beyond the upper limit of glacial sediments, bedrock is deeply weathered, as observed by means of outcropping orthogneisses. Three kilometres downstream, two right lateral moraines of Ticino glacier are preserved at elevations of 940–1000 m a.s.l. and 925–970 m a.s.l. at Premeno (Fig. 5). Near the confluence of Ticino-Toce glacier, a lateral moraine at Alpe Pala (900–910 m a.s.l.; Fig. 5) was dated to 22.9 ± 0.9 ka (VR21). Based on a serpentinite boulder indicative for the Toce catchment, it was assessed a left lateral moraine of the Toce glacier. Three kilometres ESE of Alpe Pala, two erratics from the top of Monte Cimolo (960 m a.s.l.) gave exposure ages of 25.4 ± 1.3 ka (VR23) and 22.8 ± 0.8 ka (VR24).

South of the Gulf of Borromeo, a single erratic boulder, located on the slope between Mottarone peak and Stresa at 881 m a.s.l., was dated to 70.3 ± 3.7 ka (VR19; Fig. 5). Downstream, multiple, closely spaced ice-marginal landforms can be identified on the western side of the Verbano end moraine system (Fig. 5). Right lateral moraines are preserved over an altitudinal range of more than 600 m, from Alpe Canà (830 m a.s.l.) down to the shore of Lake Maggiore (193 m a.s.l.) (Fig. 5; Fig. 6a). The number of preserved moraines decreases downstream of Poggio (Fig. 6a). Via Fosseno - Colazza - Invorio Superiore, remaining ice margins link to the frontal section of the piedmont lobe (Fig. 5; Fig. 9).

The Alpe Canà lateral moraine sequence is located above the western shore of Lake Maggiore at 830-750 m a.s.l. and is one of the best preserved glacial landscapes of the area. This extraordinary moraine set consists of up to five main lateral ridges, addressed as ridge 1–5 from oldest to youngest, respectively from west to east (Fig. 6a–d). The northern part of the Alpe Canà section is rather narrow and lacks the outermost lateral moraine. The four inner ridges stretch closely spaced over a distance of 200 m only. Spacing between the ridges increases in direction of ice flow. The largest section width (500 m) is reached where all five lateral moraines are present (Fig. 6a and b). In places, small intramorainic depressions have developed between the single ridges. With a depth of 10–25 m, the depression located between the 4th and the 5th ridge is the most prominent and continuous one of the section, even hosting a small pond (Fig. 6b and c). A major gap interrupts the

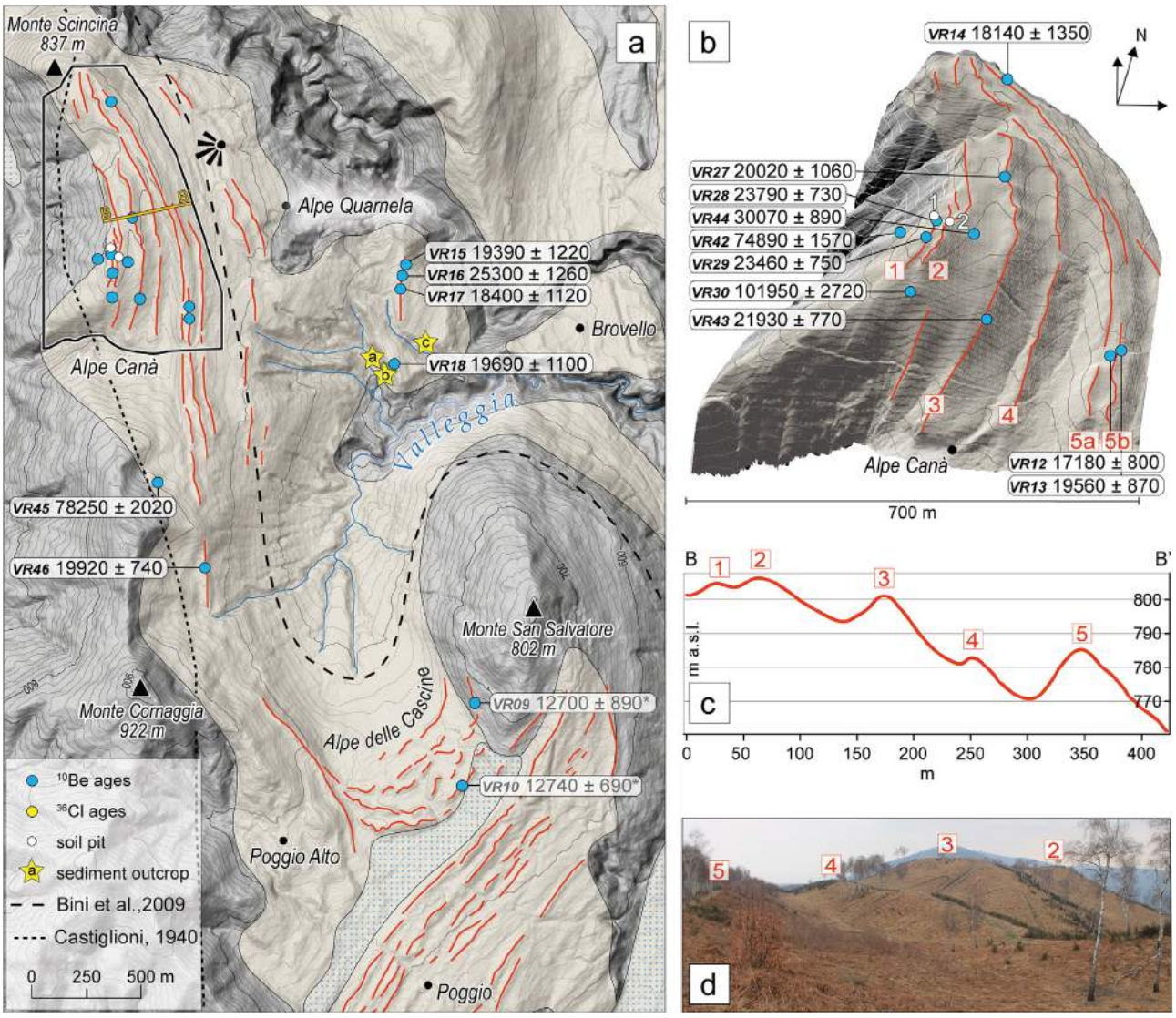

Fig. 6. LGM ice margins preserved on the right side of the Verbano piedmont lobe with gained surface exposure ages (a) (for index map see Fig. 5); (a) moraine sets between Alpe Canà and Alpe delle Cascine; yellow stars indicate locations of outcropping subglacial till (a; Fig. 8a), sequence of alternating subglacial and ice-marginal deposits (b; Fig. 8b), and glaciotectonite (c; Fig. 8c) above the town of Brovello; the viewpoint symbol indicates the approximate location of viewer standpoint in the longitudinal profile of Fig. 7; (b) 2.5D LiDAR data visualization of the Alpe Canà lateral moraine ridges, view towards N (no vertical exaggeration); (c) cross-section across Alpe Canà ice margins (vertical exaggeration is approximately 3×; for location see Fig. 6a); (d) Alpe Canà lateral moraine ridges 5–2 viewed from ridge 5 looking downglacier (ridge 1 cannot be seen in this photograph). Elevation data provided by the regional government of Piedmont (a), and the Italian National Geoportal Services (b, c). (For interpretation of the references to colour in this figure legend, the reader is referred to the Web version of this article.)

course of the Alpe Canà lateral moraines 1–4 in the upper third of the section (running meter 300–500 in Fig. 7). This opening is interpreted to have formed by a moraine breach during a glacier stage corresponding to lateral moraine 4. Another breach linked to a second glacier lobe exists at the southern end of the Alpe Canà section, where all ridges except for the innermost one (5th ridge) are disrupted. Both breaches connect to narrow and incised fluvial channels (Fig. 6a) draining towards Agogna Valley and therewith the Orta glacier system to the west (Fig. 5).

Numerous erratics are present at Alpe Canà and its southern continuation, many made of granite. Twelve boulders were selected for surface exposure dating, out of which eight are found on ridge crests. Boulder VR42 is located external to all moraines (Fig. 6a and b), 60 m downslope (west) of the outermost ridge 1. Its exposure age is 74.9 ± 1.6 ka.

The Alpe Canà external moraine 1 is a 280 m long ridge. Contrary to the pronounced inner moraines, this oldest ridge's crest is smoother and marked by less sharp slopes. The smooth character of the external moraine is especially evident where the subsequent younger moraine 2 is banked up against the inner wall of ridge 1 (Fig. 6c). At the contact of both moraines, the crests are only 20–30 m apart. A profile in a hand dug trench (Fig. 6a and b, soil pit 1), revealed 50 cm thick, weakly weathered glacial sediments above a well-developed soil. Two erratic boulders along the centre of ridge 1 were dated to 23.8 ± 0.7 ka (VR28) and 23.5 ± 0.8 ka (VR29). A massive granitic erratic sampled at the south-facing side of Alpe Canà at an intermediate position below ridge 1 and 2 yielded an age of 101.9 ± 2.7 ka (VR30; Fig. 6a and b).

The adjacent inner lateral moraine 2 is preserved over a length of 900 m. No erratics were found along the crest, but a boulder on the inner slope of moraine 2 was dated to 30.1 ± 0.9 (VR44). In a hand dug shallow pit (Fig. 6a and b, soil pit 2), sediments showed

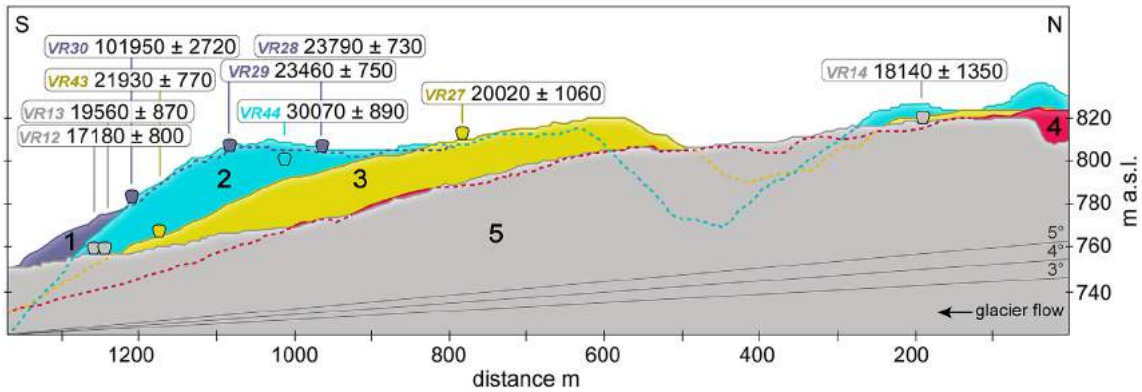

Fig. 7. Projected longitudinal profile (N–S extension) of the five Alpe Canà lateral moraine ridges viewed from the inner towards external ice margin. Approximate location of viewer standpoint is shown in Fig. 6; view is to the west. Vertical exaggeration is approximately 3×. Locations and exposure ages (a) of dated erratic boulders are shown, the colours of the filled symbols correspond to the moraine attributions (for details see text). LiDAR elevation data provided by the Italian National Geoportal Services. (For interpretation of the references to colour in this figure legend, the reader is referred to the Web version of this article.)

weak signs of weathering. South of Alpe Canà, distinct lateral moraines are poorly preserved, except for the innermost lateral ridge 5. In the hypothetical continuation of ridge 1–2 scattered glacial sediments cover slopes up to about 820 m a.s.l. Here a massive, well-rounded erratic boulder at 795 m a.s.l. yielded an exposure age of 78.3 ± 2.0 ka (VR45; Fig. 4c; Fig. 6a). Although VR45 is in topographic continuation of Alpe Canà ridge 1–2, the geomorphological situation is not entirely clear.

The inner Alpe Canà ice margins 3–5 are more continuous compared to the external ridges. Preserved over a length of 1.2–1.3 km the lateral moraines overcome a vertical distance of 70 m (Fig. 7). In the lower part of the Alpe Canà section, moraine ridge 5 splits up into two distinct ridges, 5a and 5b (Fig. 6a and b). While the lower ridge 5b fades out after 500 m, ridge 5a continues on for an additional 2 km. It is the only Alpe Canà ice margin that can be traced past the frontal moraines of Alpe delle Cascine, down to just east of the town of Poggio Alto (Fig. 6a). A post-depositional slope failure at the eastern slope of Monte Cornaggia (Fig. 6a) might however have destroyed evidence of more external ridges. From moraine ridge 3, two exposure ages were determined to 20.0 ± 1.1 ka (VR27) and 21.9 ± 0.8 ka (VR43). Boulder VR27 is only 1 m above the ground. Compared to VR43, its younger age suggests it was temporarily covered by sediment. Due to the absence of suitable erratic boulders no exposure ages could be determined for moraine 4. Four exposure dates are available for the innermost Alpe Canà ridges, 18.1 ± 1.4 ka (VR14) for ridge 5, 19.9 ± 0.7 ka (VR46; Fig. 4d; Fig. 6a) for ridge 5a, and 17.2 ± 0.8 ka (VR12) and 19.6 ± 0.9 ka (VR13) for ridge 5b (Fig. 6a and b). The age of VR12 yields a younger exposure age in comparison to VR13, VR14, and VR46 that overlap within their uncertainties. This 'too young' age is likely due to the low height above ground (80 cm). In contrast, sample VR46 stems from an impressive erratic boulder spanning 8 m across the crest of moraine 5a. Due to its wide, embedded base and large dimensions, we assume that boulder VR46 (19.9 ± 0.7 ka) best reflects the depositional age of lateral moraine complex 5.

The Alpe delle Cascine frontal moraines are confined in a minor valley bounded by the peaks of Monte Cornaggia (922 m a.s.l.) and Monte San Salvatore (802 m a.s.l.) and consist of five closely spaced frontal moraines (Fig. 6a). The arcuate terminal moraines are found at 645-630 m a.s.l. Single ridges are up to 400 m long and 15 m high, while most moraines are only a few meters in height and, due to frequent dissection, much shorter. In the centre of the small amphitheatre a 20 m wide meltwater outlet is evident. Upglacier of Alpe delle Cascine, a U-shaped glacial basin, not more than 800 m wide and 1 km long is found. The basin's smooth valley floor today is gradually captured by the headwaters of Valleggia Creek draining north towards Brovello. This depicts a 180° shift in draining direction compared to the time of Alpe delle Cascine moraine deposition. Based on altitudinal and geomorphological relationships, we correlate the frontal moraines of Alpe delle Cascine and the adjacent set of right lateral moraines above Poggio village (Fig. 6a) to the weakly preserved lateral moraines between Alpe Canà and Alpe Quarnela (Fig. 6a). Located 20–60 m below the crest of Alpe Canà ridge 5 (775 m a.s.l.), these ice margins remain vague due to agricultural practices (Fig. 6a). Two exposure ages calculated from the Alpe delle Cascine frontal moraine set (12.7 ± 0.9 ka (VR09); 12.7 ± 0.7 ka (VR10)) unfortunately yield insufficient age control. A wealth of data supports the conclusion that by that time glaciers were long withdrawn from the foreland (Bernoulli et al., 2018; Ivy-Ochs et al., 2008; Reber et al., 2014; Scapozza et al., 2014; van Husen, 1997). The calculated ages are hence believed to have been distorted by human impact, post-depositional exhumation, or destabilization of the respective erratic boulder.

Above the town of Brovello, one last moraine ridge parallel to the Alpe Canà lateral moraines was identified at 570-560 m a.s.l. (Fig. 6a). From the wide and rather flat moraine ridge, rich in big erratic boulders, four exposure ages were determined to 19.4 ± 1.2 ka (VR15), 25.3 ± 1.3 ka (VR16; Fig. 4a), 18.4 ± 1.1 ka (VR17), and 19.7 ± 1.1 ka (VR18). Three out of four boulders dated on this moraine ridge yield similar ages within their uncertainties (VR15, VR17, VR18). Solely sample VR16 holds a significantly older exposure age (25.3 ± 1.3 ka). We hence suppose that this boulder experienced a complex history, likely including exposure prior to reaching its present position. In light of the local situation and the boulders' appearance, the exposure ages of VR15 (19.4 ± 1.2 ka) and VR18 (19.7 ± 1.1 ka) are interpreted to best represent moraine stabilization time.

Significant outcrops of glaciogenic deposits are distributed above Brovello due to the presence of deep incisions and road cuts (Fig. 6a, outcrop a-c; Fig. 8a–c). Under the Brovello moraine on which boulder VR18 lies, the incision of a small tributary to the Valleggia stream exposes a vertical, 30 m thick, sequence of subglacial and ice-marginal deposits at approximately 530–560 m a.s.l. (45.841327° E, 8.520912° N). At the bottom of the sequence an isolated outcrop in the stream thalweg at ca. 530 m a.s.l. shows a 2.5 m thick, massive, overconsolidated matrix-supported diamicton made up of blue-grey fine sand and silt (Fig. 6a, outcrop a; Fig. 8a). The proportion of clasts is about 5%. The clasts are centimetre-sized, faceted, and striated. Some of them are oriented along thrust surfaces that dip 115/35. A single 20 cm long cobble as

Fig. 8. Sediment outcrops above the town of Brovello (for locations see Fig. 6a and section 4.1): (a) subglacial till; (b) stratified, ice-marginal delta deposit below submarginal till; (c) glaciotectonically deformed ice-marginal deposits. Hammer for scale (a, c).

maximum size is present. This deposit is interpreted as subglacial till deposited during the formation of the overlying Alpe Canà ice-marginal sequence. A few metres higher, a matrix-supported diamicton, interpreted as subglacial melt-out till, crops out at the base of an extensive vertical cliff. Year round vegetation cover hides the transition to the above thinly stratified sands of at least 5 m thickness (Fig. 6a, outcrop b; Fig. 8b). The sandy layers show an apparent inclination of 10° and dip towards 150. Nearby, similar clinostratified sands were found only partially exposed but as low as 500 m a.s.l. Above a roughly 10 m thick, alternating sequence of fine sands and gravel layers, deposited with a steeper angle of 20–25°, follows (Fig. 8b). This sequence likely originates from the early re-sedimentation of glaciogenic deposits eroded along the slope below Alpe Canà. Deposition in an ice-marginal delta-fan is indicated by well-sorted and clinostratified deposits. At the top of the sequence (ca. 555–560 m a.s.l.), a 5 m thick matrix-supported diamicton with larger clasts is exposed. Forming the top of the overlying Brovello moraine, it is interpreted as readvance submarginal till.

Downslope of the Brovello moraine, a road cut exposes ice-marginal sediments over a length of 30 m (Fig. 6a, outcrop c; Fig. 8c; 45.841956° E, 8.523210° N; ca. 530 m a.s.l.). The section shows a deformed sequence of clast-free sand layers and matrix-dominated lenses rich in clasts. Locally thin and discontinuous diamicton lenses are folded within sand layers. Clasts are sub-angular, reach up to 20 cm in size, and are characterized by erratic lithologies. Folding and thrusting (dipping N100/20) affect different layers and suggest syn- and post-depositional compressive stresses. Deformation is interpreted to have occurred at the bed of the readvancing Ticino-Toce glacier with the glacier margin located at the nearby Brovello moraine (erratic boulders VR15-18). We hence argue that the deposit should be addressed as glaciotectonite (Evans, 2007) derived from ice-marginal delta-fan deposits.

Multiple lateral moraines connect the western ice margins to the frontal section of the piedmont lobe (Fig. 5). Banked up against the bedrock ridge of Motta dell'Arbigiera (677 m a.s.l.), several lateral moraines are preserved between Fosseno and Colazza, starting 1 km downstream of Poggio (Fig. 9). The moraines are several hundred meters long and reach up to the summit of Motta dell'Arbigiera. The outermost and highest ice margin preserved in the Fosseno-Colazza moraine set consists of two ridges and was dated to 23.3 ± 1.3 ka (VR05) and 25.0 ± 0.9 ka (VR31). The latter erratic is regionally known as Sass Preiatecia or Sasso del Diavolo, a ~20 m^3 large boulder made of orthogneiss of the Serie dei Laghi (VR31; Fig. 4b). On top of a 40 m lower internal moraine, three more erratic boulders were exposure dated to 15.8 ± 1.9 ka (VR06), 18.5 ± 1 ka (VR07), and 25.5 ± 4.3 ka (VR33). A road cut through this moraine north of Colazza exposes an ice-marginal flow till rich in decimetric-sized clasts in a sandy matrix. Based on the elevations and trends of moraine fragments, as well as the fact that there is no evidence of an external ice margin at either site, we correlate the moraines between Fosseno and Colazza to the Alpe Canà moraine complex. The innermost ice margin above Colazza (600-565 m a.s.l.) turns southwards and ends after about 3 km just north of Invorio Superiore (485 m a.s.l.). This moraine ridge is undated due to lack of erratic boulders suitable for exposure dating but assumed to have been deposited shortly after its external counterpart.

East of Invorio Superiore (Fig. 5), at the transition to the frontal sector of the end moraine system, a bedrock high (511 m a.s.l.; Massiccio dei Laghi; Piana et al., 2017) is covered with glacial sediments with suggestions of broad indistinct ridges. On site, three erratics were dated to 19.2 ± 0.9 ka (VR01), 19.9 ± 2.7 ka (VR02), and 20.6 ± 1.2 ka (VR03). Located between 460-490 m a.s.l., exposure dates provide minimum ages for deglaciation of the hill top. Based on the elevations of the preserved right lateral moraines to the

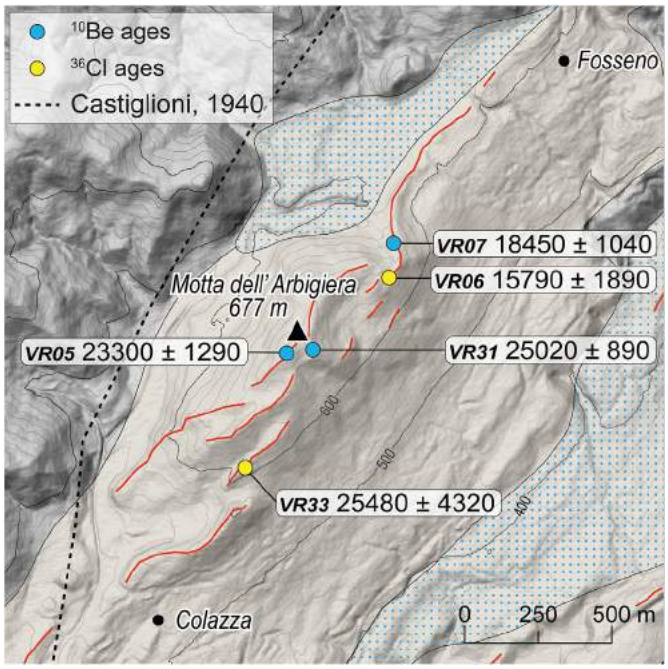

Fig. 9. Multiple generations of lateral moraines on the western part of the Verbano end moraine system between Fosseno and Colazza with surface exposure ages (a). For index map see Fig. 5. Elevation data provided by the regional government of Piedmont.

south and west (Fig. 5), the hill top likely became ice free before the deposition of Alpe Canà moraine ridge 5 at 19.9 ± 0.7 ka, which agrees well with the ages of VR02 and VR03.

4.2. Eastern sector

Investigated sites in the eastern part of the Ticino-Toce piedmont glacier can be grouped into two main areas: (1) the mountain group confined by Lake Maggiore to the west and Valcuvia Valley to the east in the northern part of the study area (Fig. 5); and (2) to the south, the prominent lateral moraine ridges preserved on the W and SW slopes of Monte Campo dei Fiori (1225 m a.s.l.) between the Valcuvia Valley outlet and the town of Varese (Fig. 5; Fig. 10).

On peaks enclosed by the Lake Maggiore basin and Valcuvia Valley along the eastern side of Ticino Valley, glacial sediments were observed at altitudes well above 1000 m a.s.l. Patchy till is present on the wide summit of Monte Pian Nave at 1060 m a.s.l. (Fig. 5). An erratic boulder (VR36) at 1038 m a.s.l. was dated to 17.3 ± 0.8 ka. Two kilometres further south, single erratic clasts reach up to 1000–1010 m a.s.l. on the northern slopes of Monte della Colonna (1200 m a.s.l.) and to the top of Pizzo di Cuvignone (1010 m a.s.l.). On the northern slopes of Sasso del Ferro (1060 m a.s.l.), the southernmost peak of the mountain range, large erratic boulders are present at elevations of 870 m a.s.l. In contrast, no erratic boulders were observed between 900 and 830 m a.s.l. on a plateau SE of Sasso del Ferro.

A limestone ridge thinly covered with glacial sediment is protruding 350-250 m above the present-day Valcuvia Valley floor at 280 m a.s.l. (Fig.5; Fig. 10). A single erratic (VR41) on the northeastern end of the bedrock ridge was exposure dated. The result of 15.8 ± 0.6 ka suggests that this erratic was initially buried. The age is consequently interpreted as minimum age for boulder deposition. As discussed in more detail below, absolute ages from several upstream sites (Bernoulli et al., 2018; Scapozza et al., 2014) suggest that glaciers had long retreated from the foreland by that time.

Further downstream, along the slopes of Campo dei Fiori, the highest glacial sediments were found at 800 m a.s.l. west of the corresponding peak (Fig. 10). From here patchy deposits of an outer lateral moraine can be followed for 7 km along the SW-facing mountain slopes down to 520 m a.s.l. South of Velate the ice margin ceases in the outskirts of Varese. Erratic boulder ages from the northern edge of this ice margin (Fig. 10) were determined to 23.2 ± 0.8 ka (VR54) and 25.0 ± 0.7 ka (VR55). A few tens of meters lower ice margin with maximum elevation of 730 m a.s.l., is marked by a prominent, up to 40 m high, steep-sided lateral moraine. This ridge and its branch offs represent the innermost consecutive ice margin preserved in the eastern part of the Verbano lobe. Strongly bent and steeply inclined (ca. 10%), the upper stretch of the moraine ridge marks the exit angle of the Valcuvia glacier branch (Fig. 10). Well preserved within the Campo dei Fiori Regional Park, the lateral moraine continues with an inclination of 3–3.5% parallel to the mountain slope for about 4 km until 560 m a.s.l. north of Chignolo (Fig. 10). Three boulders dated along this innermost moraine yielded ^{10}Be exposure ages of 19.4 ± 0.5 ka (VR49), 19.8 ± 0.7 ka (VR50), and 21.8 ± 0.6 ka (VR53). Over half of the distance the lateral moraine is accompanied by a contiguous second ridge that runs parallel in an external position. Multiple shorter and closely spaced lateral moraine ridges and a kame terrace are additionally banked up to the slope and build a continuum to the outer ice margin (Fig. 10). Dissected by stream channels and overprinted by human settlements, disintegrated inner ice margins can be followed as far as the agglomeration of Varese (Fig. 10) from where they connect to the frontal sector of the amphitheatre. Road cuts through and along the lateral moraines expose sandy, matrix-supported diamictons that are rich in subangular to subrounded faceted clasts of various sizes and made up of local limestones and erratic crystalline lithologies. Inside the Campo dei Fiori Park, erratic boulders up to several cubic meters in size are frequently found on the moraine surfaces.

4.3. Frontal sector

The frontal ice margins of the Verbano amphitheatre can be grouped into a western part with good landform preservation and multiple terminal moraines ridges that are traceable for several kilometres, and an eastern sector with more strongly dissected ridges and ambiguous links across them. The boundary between the two areas roughly coincides with the stream course of Ticino River and the regional border between Piedmont and Lombardy.

Emerging from the right side of the end moraine system, a set of well-preserved frontal moraines spans discontinuously over a distance of 14 km from Invorio Superiore via Gattico and Borgo Ticino towards the breach of Ticino River (Fig. 5). In parts, this moraine set consists of pronounced, tens of metres high ridges. In other places the ice margin appears wider and flatter and is characterized by numerous moraine fragments of minor height. Along this terminal ice margin, two prominent serpentinite boulders, locally known as Sass Malo 1 km southeast of Gattico (VR51; Fig. 4e) and Prea Guzza 2 km northwest of Borgo Ticino (VR52; Fig. 4f) were ^{36}Cl dated to 27.6 ± 7.8 ka and 25.6 ± 3.3 ka, respectively. Erratic VR51 is situated at 336 m a.s.l. on the crest of the outer of two prominent and closely spaced frontal ridges. Four kilometres further to the SE, the latter boulder rests on a low proglacial terrace a few hundred meters external to the described ice margin. A fragmented and single ridged intermediate ice margin resides 1 km internally to the main ice position identified. Separated by a former meltwater channel, that is presently only occupied by a small stream, a third moraine complex follows roughly 2 km behind the external moraine set (Fig. 5). This innermost ice margin consists of one to four ridges. With remarkable sinuous trend, ice-marginal landforms arch from the town of Oleggio Castello towards Ticino River before fading away after 9 km (Fig. 5). Overconsolidated diamictons were observed within these end moraines. In absence of suitable erratics, no surface exposure ages could be derived for the two inner ice margins. In parts, moraines were reworked by fluvial cut and fill processes. A distinct terrace level related to each of the three frontal moraine sets described above can be recognized along Ticino River and at a former meltwater outlet southeast of Gattico (Piana et al., 2017).

From the eastern side of the amphitheatre, a prominent but strongly fragmented and anthropogenically overprinted ice margin runs in an arc from the agglomeration of Varese southwestwards to Azzate (Fig. 5). In parts, this ice margin appears as a distinct double ridge and reaches maximum elevations of 375-400 m a.s.l. Westwards from Azzate weakly weathered ice-marginal deposits continue along a concave NE-SW trajectory following inselbergs made up of Eocene limestones and Oligocene conglomerates and sandstones (Mattirolo et al., 1932; Carte geologiche Varese - Litologica e Mineraria, 1:10′000; cartografia.provincia.va.it). Contrary to the western and eastern sectors described above, distinct multiridged moraine sets are not apparent in this part of the study area. Glacial sediments and erratic boulders were however observed on hill tops west of Monte Rogorella (Fig. 5) at 400 m a.s.l. Glacial cover up to similar elevations is likewise indicated for adjacent bedrock structures (Mattirolo et al., 1932; Carte geologiche Varese - Litologica e Mineraria, 1:10′000; cartografia.provincia.va.it). Recurring

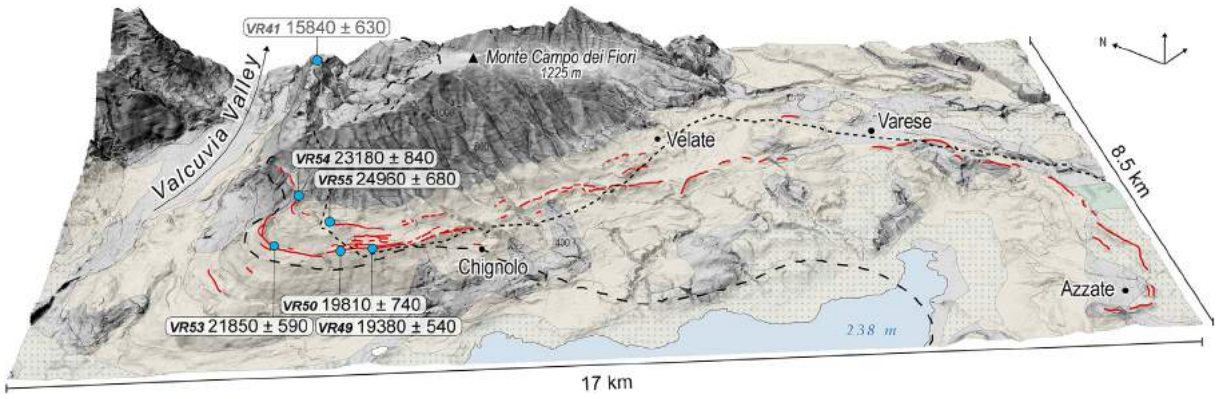

Fig. 10. Lateral moraine ridges preserved along the slope of Monte Campo dei Fiori and their transition to the former LGM glacier front at Varese and Azzate, view towards the NE (vertical exaggeration: 2×). ^{10}Be exposure ages (a) indicate LGM origin of ice-marginal deposits up to 800 m a.s.l. For index map see Fig. 5. Elevation data provided by the regional government of Lombardy.

south of the bedrock lineament, frontal moraines connect to the ice margin on the Piedmont part of the moraine system via the town of Sesona (Fig. 5). In external positions, deposits are more deeply weathered (Bini, 1997; Bini and Zuccoli, 2004), moraine ridges are flatter, more strongly oriented N–S, and cross-cut by younger moraines (e.g. around Azzate). Along the Verbano frontal moraines erratic boulders are rarely preserved. Unfortunately, no erratic was found suitable for exposure dating in the southeastern part of the end moraine system.

5. Discussion

5.1. Reconstruction of extent and timing of the Ticino-Toce glacier

Geomorphological investigations paired with surface exposure dating were applied for detailed reconstruction of timing and extent of the last Ticino-Toce paleoglacier. Frequently available erratic boulders allowed to date the full range of preserved lateral moraines on both sides of the Verbano end moraine system. Even minor paleoglacier fluctuation could thereby be chronologically constrained.

In our study we obtained five ages (70.3 ± 3.6 ka (VR19), 101.9 ± 2.7 ka (VR30), 74.9 ± 1.6 ka (VR42), 30.1 ± 0.9 ka (VR44), and 78.3 ± 2.0 ka (VR45)) that predate the LGM (Table 1). We consider these to be minimum ages (Briner et al., 2005; Heyman et al., 2011; Putkonen and Swanson, 2003), perhaps related to a glacier expansion during MIS 6. Respective samples all stem from the western side of the end moraine system, between the Gulf of Borromeo and Alpe Canà (Fig. 5; Fig. 6a and b). Chronological data combined with soil pit information (section 4.1) suggest that older ice margin(s) were apparently buried underneath the LGM ice margin. The combined evidence points to re-occupation of previously constructed right lateral ice margins during the LGM. Thus, earlier foreland reaching glaciation(s) had lateral extents comparable to those of the last glaciation. Boulders VR30, VR42, VR44, and VR45 are all situated on slopes not on moraine crests, underpinning our hypothesis that they were deposited during a pre-LGM glaciation and were subsequently exhumed. Considering the fact that these pre-LGM boulders protrude from the present-day surface, LGM cover sediments may have been rather thin.

Spatial relationships of lateral and terminal moraines show that the LGM Verbano lobe extended from the outermost moraine of Alpe Canà (Fig. 6) south to Fosseno, Colazza, and Invorio Superiore (Fig. 9). Via Gattico, and Borgo Ticino (Fig. 5), the LGM ice margins continue eastwards to Varese and the higher Campo dei Fiori lateral moraine (Fig. 10). Consistent maximum ages along this ice margin (VR31, VR55) point to LGM glacier stabilization at 25.0 ± 0.9 ka (Fig. 11a). Two samples (VR51, VR52) from the paleoglacier front between Gattico and Borgo Ticino confirm this timing. Despite lack of exposure dates in the eastern frontal part of the piedmont lobe, pronounced moraine ridges and their weakly weathered glacial sediments found in the projection of confirmed LGM ice margins allow the reconstruction of the full width of the LGM glacier lobe. The eastern part of the Ticino-Toce glacier lobe advanced beyond todays Lake Varese, Lake Comabbio, and Lake Monate (Fig. 11a).

Between Borgo Ticino and Azzate, the glacier front possibly remained 3 to 6 km behind LGM terminal moraines adjacent to the east and west (Figs. 5 and 11a). In this sector the terminus of the glacier was likely affected by the presence of narrow bedrock ridges. With altitudes up to 400–430 m a.s.l., the inselbergs reach similar heights as nearby LGM terminal moraines and must have been significant obstacles to glacier flow. We assume that the bedrock barrier blocked and split the LGM Ticino-Toce glacier and locally prevented it from spreading further onto the Po plain. Glacial sediments and erratic boulders found on top of the inselbergs indicate that the glaciers had either overtopped them or resided behind them, dumping glacial material on top of the bedrock highs. This setting may have hindered the accumulation of a multi-ridged moraine set found in other places along the LGM front. Not being able to overtop the described bedrock ridges, Ticino-Toce glacier likely did not form a single symmetric piedmont lobe during LGM. Instead, an up to 16 km wide western glacier lobe may have developed. A second lobe of minor width (6 km) formed to the east (Fig. 11a). Compared to the eastern lobe, the western lobe advanced several kilometres further onto the foreland. This may be linked to present altitudinal differences. Main glacier flow was most likely concentrated along the basin of Lake Maggiore rather than the slightly elevated area to the east.

More extensive older glaciations must not have been affected by the bedrock highs, and the consequential development of two glacier lobes, in similar ways. That Ticino-Toce glacier was able to advance beyond the bedrock ridges in the past is indicated by the lobate-shaped ice margins preserved in external positions to the LGM terminal moraines between Somma Lombardo and Azzate (Fig. 5; Bini, 2012).

In the northern part of the study area, gained exposure ages and field observations allow clear constraints on LGM ice surface height. Exposure ages from Monte Pian Nave, 9 km upstream from Laveno (Fig. 5), show that LGM Ticino glacier reached at least up to 1040 m a.s.l. Most probably the mountain top (1060 m a.s.l.) was

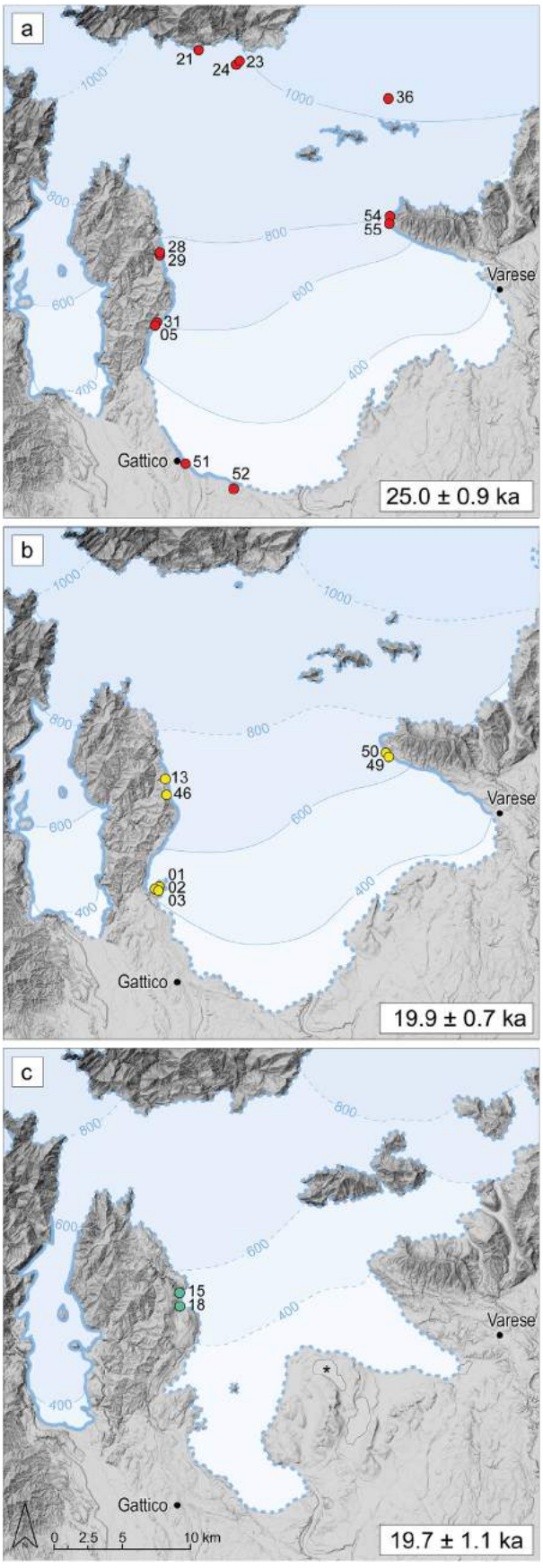

Fig. 11. Reconstructions of the Verbano lobe of the Ticino-Toce paleoglacier during (a) LGM maximum advance (25.0 ± 0.9 ka), (b) an inner LGM position (19.9 ± 0.7 ka), and (c) a late LGM readvance (19.7 ± 1.1 ka). Contour lines of the ice surface were reconstructed based on dated ice margins. The asterisk in Fig. 11c marks a minimum age for deglaciation of today's Lake Monate of 19.9–18.8 ka cal BP (Rey et al., 2020). Reconstruction of the Orta lobe based on Braakhekke et al. (2020). Elevation data provided by the regional governments of Piedmont and Lombardy.

completely covered by ice. In light of the Monte Pian Nave age, we argue that glacial sediment limits observed in similar range on other slopes of the mountain group, as well as above Gonte (Fig. 5), are likewise indicative of the LGM ice level. This assumption is in good agreement with the dated Alpe Pala ice margin at 900–910 m a.s.l. and the exposure ages from Monte Cimolo (960 m a.s.l.) at the confluence of Toce and Ticino paleoglacier (Fig. 5). The LGM ice level lowered to 800 m a.s.l. at the inflow of Valcuvia glacier branch (Fig. 11a). With maximum ages of 25.4 ± 1.3 ka to 22.9 ± 0.8 ka, the chronological data from the confluence zone is numerically consistent with LGM maximum ages from the end moraine system.

Small-scale glacier fluctuations during the LGM maximum are well documented on both sides (Alpe Canà, Fosseno-Colazza, Campo dei Fiori) and the front of the end moraine system. Over the majority of the LGM maximum phase, glacier oscillations caused only minor reductions in ice level (few tens of metres) and frontal extent (few hundreds of metres). Exposure ages from Alpe Canà, where chronological constraints are the most robust, suggest stabilization of a new ice margin roughly every 1000 years (ridge 1, 23.8 ± 0.7 ka; ridge 3, 21.9 ± 0.8 ka; ridge 5, 19.9 ± 0.7 ka). In analogy to Alpe Canà, on the left side of the former glacier lobe, multiple parallel but minor ice margins (lacking boulders suitable for surface exposure dating) are preserved at Campo dei Fiori (Fig. 10). Only the higher (25.0 ± 0.7 ka) and lower lateral (19.8 ± 0.6 ka) moraines are dated on site; their ages cover the same time frame as the Alpe Canà complex. A prominent bend in the lower Campo dei Fiori lateral moraine marks the outflowing Valcuvia glacier branch of Ticino glacier. This high, steep-walled lateral moraine (up to 40 m) might have been reoccupied, with initial construction at 21.8 ± 0.6 ka as suggested by the age of boulder VR53.

Around 19.9 ± 0.7 ka, Ticino-Toce glacier snout was located slightly behind its LGM maximum position, at an intermediate ice position identified between the terminal moraine sets of Gattico and Oleggio Castello (Fig. 5; Fig. 11b). The onset of this recession is indicated by proceeding deglaciation of a hilltop east of Invorio Superiore (directly behind and at similar altitudes as the LGM maximum moraines of Invorio Superiore; Fig. 5) around 20.6 ± 1.2 ka to 19.9 ± 2.8 ka. The internal LGM maximum stand itself is perhaps related to the prominent inner ice levels of Campo dei Fiori and Alpe Canà (ridge 5) that show similar character. The marginally lowered lateral ice margins and slightly reduced frontal extent reconstructed for the western part of the lobe likely did not affect the overall shape of the piedmont glacier (Fig. 11b). Based on the consecutive lateral moraine ridges between Alpe Canà and Poggio (Fig. 6a), an ice surface slope of 4.5% is reconstructed for this late LGM glacier. On the right side of the Verbano lobe, topographic constraints extend down to Invorio Superiore. Along the eastern glacier margin bedrock constraints end further upstream with Monte Campo dei Fiori (cf. Fig. 5). Due to this disparity, the glacier's surface angle is not only expected to decrease towards the glacier front with increasing glacier width but also gradually towards the east.

After a ca. 5000-year long period of minor glacier oscillations, the onset of glacier retreat is marked by the withdrawal from the innermost Alpe Canà (moraine ridge 5; Fig. 6a) and Campo dei Fiori ice margin (Fig. 10) after 19.9 ± 0.7 ka and 19.8 ± 0.7 ka, respectively. A stepwise glacier thinning rather than a collapse of the glacier tongue is suggested by the geomorphological record on the

right slopes of the Verbano amphitheatre. The multiple moraine ridges at Alpe delle Cascine and above Poggio (Fig. 6a) allow to reconstruct a progressively thinning glacier with frequent phases of stabilization. While vertical changes in ice surface height are well mimicked, corresponding extents of the glacier front are not recorded in equal detail. With continuing lowering of the ice surface, slope material from Alpe Canà was mobilized and deposited in an ice-marginal lake as shown by glaciolacustrine foreset beds along a Valleggia tributary (Fig. 6a; Fig. 8b). Delta aggradation ceased as a consequence of glacier readvance that led to the deposition of a last glacial till on top of the glaciolacustrine sequence. Nearby glaciotectonically deformed ice-marginal sediments (Fig. 8c) independently suggest that the Ticino-Toce glacier on site temporarily retreated below 600 m a.s.l. (>200 m relative to LGM maximum stand) and later readvanced.

While the sedimentological evidence for a LGM readvance of the glacier is quite strong, information on its extent and therefore also timing is less straightforward. Which ice margin relates to the readvance stadial cannot be resolved entirely as multiple moraines are present above Brovello, including the Alpe Canà ridges (Fig. 6a). However, it seems unambiguous to connect the ice margin directly overlying the till with the glacier readvance. If so, readvance of the Ticino-Toce glacier would have happened no later than 19.7 ± 1.1 ka as indicated by exposure ages from the Brovello moraine. The cycle of glacier retreat and subsequent readvance would consequentially have had to have happened in a comparatively short time frame between 20.6 ka and 18.6 ka, when one takes into account associated age uncertainties. In fact, the exposure ages of the ice margins accumulated prior to glacier retreat (Alpe Canà ridge 5 at 19.9 ± 0.7 ka) and during the readvance (ice margin above Brovello at 19.7 ± 1.1 ka) overlap within uncertainties. The Brovello moraine depicts only a small remnant of a former ice margin. No continuing ridge can be followed towards the former glacier snout. Based on geomorphological and altitudinal relationships however, the innermost identified ice margin at Oleggio Castello at the southern tip of today's Lake Maggiore could represent the analogue frontal deposits to the ice-marginal relict above Brovello, but lacks direct age constraint. This would mean that during this late LGM readvance a 240 m lower ice surface was associated with an approximately 2 km shorter frontal ice margin, in comparison to the LGM maximum extent. For the eastern sector of the lobe, the extent of the readvance remains vague due to discontinuous geomorphological evidence and the lack of chronological information.

5.2. New chronological and spatial evidence for the LGM of the Ticino-Toce glacier in relation to previous reconstructions

In absence of numerical chronological data, different suggestions on the number and extent of glaciations within the Verbano amphitheatre have been put forward (Bini et al., 2009; Castiglioni, 1940; Hantke, 1983; Penck and Brückner, 1909). This study explores the role of the last glacial cycle for the build-up of the Verbano end moraine system by means of surface exposure dating and landform analysis. For the first time the LGM advance of the Ticino-Toce glacier system was successfully constrained to 25.0 ± 0.9 ka to 19.9 ± 0.7 ka (Fig. 13).

The new chronological evidence further confirms that large parts of the Verbano amphitheatre were built during the Last Glacial Maximum. This novel insight is in contrast to recent interpretations that had (a) supported a significantly smaller LGM glacier extent (Fig. 2a; Bini et al., 2009) and (b) related the LGM terminal moraines identified in this study to different Middle Pleistocene glaciations (Bini, 2012; Bini et al., 2014). The here presented LGM reconstruction (Fig. 11a) markedly exceeds previous maps (Bini et al., 2009) by nearly 200 km^2 in area and several kilometres in glacier extent. Our results prove that today's intramorainic lakes were completely covered by ice during the peak of LGM, differently to earlier assumptions (Bini et al., 2009). Based on our reconstructions the LGM piedmont lobe was further not shaped as uniform as suggested by early authors (Fig. 2b–d; Castiglioni, 1940; Hantke, 1983; Jäckli et al., 1970; Penck and Brückner, 1909). Along the final Ticino Valley stretch, between Luino and Laveno (Fig. 5), the ice surface of the advancing LGM Ticino glacier reached above 1000 m a.s.l. Local LGM ice levels, were previously estimated to be 150–200 m lower (Bini et al., 2009; Hantke, 1983).

The moraine set of Oleggio Castello had previously been assigned to the main LGM advance (Bini, 2012; Bini et al., 2009) or to the first post-LGM recessional stadial of the Ticino-Toce glacier (Sesto Calende stadial; Hantke, 1983). This study suggests deposition during a late LGM glacier readvance (Fig. 11c). Based on altitudinal relationships, the Oleggio Castello frontal moraine complex could represent the counterpart to the readvance (lateral) moraine above Brovello, dated to 19.7 ± 1.1 ka. Due to incomplete preservation of the geomorphological record on the steep slopes above Lake Maggiore, it cannot be said with absolute certainty that both ice margins belong to the same stadial. Nevertheless, a late LGM depositional age of the Oleggio Castello terminal moraines is certain given the relative position internal to the LGM terminal moraines. How far the readvancing glacier front reached in the eastern sector of the lobe remains unclear (Fig. 11c). Lake sedimentation at Lake Monate (Fig. 5) set in at 19.9–18.8 ka cal BP (Rey et al., 2020). Ice free conditions at Lake Monate could be correlated with either the Ticino-Toce glacier residing upstream of the lake during its readvance or the collapse of the piedmont glacier in the phase of early Lateglacial ice decay. Lack of preserved ice margin in the area between Lake Maggiore and Lake Varese does not allow distinct conclusions.

The presented dataset constrains the onset of glacier downwasting to have occurred just after 19.7 ± 1.1 ka. Onset of lake sedimentation at Lake Monate shows that the final readvance of Ticino-Toce glacier must have been short-lived and the collapse of the piedmont glacier was underway by 19.9–18.8 ka cal BP (Rey et al., 2020). Amplified by a calving front (Scapozza et al., 2012), early Lateglacial ice decay of Ticino-Toce glacier is believed to have occurred rapidly within 1000–1500 years as was shown for other large glacier systems in the Alps (Reitner, 2007; Rey et al., 2020).

5.3. Comparison of the LGM Ticino-Toce and Toce glacier systems in Verbano and Orta amphitheatres

Downstream of Ossola Valley, Toce glacier diverged into two branches. While one branch continued southeastward to merge with the Ticino glacier system a second branch advanced directly to the south to fill the comparatively narrow and confined Orta basin (Figs. 2a and 12). The thereby formed Orta amphitheatre is made up of three moraine belts, all of them recently assigned to LGM by means of surface exposure dating (Braakhekke et al., 2020), plus more external older glacial deposits. The LGM maximum in the Orta end moraine system was defined as the time range between 26.5 and 23 ka (Fig. 1; Table 4; Braakhekke et al., 2020) and compares well to ages determined for the most external LGM ice margins of the Verbano lobe (25.0 ± 0.9 ka to 23.8 ± 0.7 ka). One respectively two internal moraine belts characterize both, the western section of the Verbano amphitheatre and the Orta amphitheatre (Fig. 6b in Braakhekke et al., 2020). In each case, the interior moraine sets are located one to 2 km behind their LGM maximum ice margin. Made up of multiple closely spaced ridges, both inner stadials suggest an oscillating glacier front. Sedimentological evidence from the Verbano lobe allowed identifying this stadial as glacier readvance. As the sediments along the western side of the Verbano system

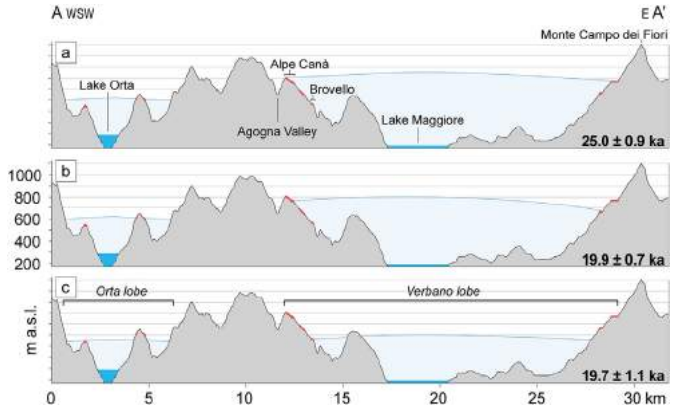

Fig. 12. Cross-sections through the two outlets of the Ticino-Toce glacier system, Orta (Braakhekke et al., 2020) and Verbano lobes, over the course of the LGM (a–c).- Preserved moraine ridges (e.g. between Alpe Canà and Brovello; the two main ice margins on the SW slope of Monte Campo dei Fiori) are highlighted in red. Present-day Lake Orta and Lake Maggiore (bedrock lake floor not shown) are indicated in blue. Vertical exaggeration is approximately 30×. Position of the cross-sections is indicated in Fig. 5 (A-A'). Elevation data provided by the regional governments of Piedmont and Lombardy. (For interpretation of the references to colour in this figure legend, the reader is referred to the Web version of this article.)

originate from the Toce glacier branch, a readvance character is also suggested for the Orta inner moraine set, which was previously discussed as a stabilization phase or readvance (Braakhekke et al., 2020). Depositional ages for this late LGM readvance stadial, determined to 19 ± 1 ka for the Orta catchment (Braakhekke et al., 2020) and 19.7 ± 1.1 ka for the Verbano lobe, are in good agreement which each other. Concordant ages point towards similar climate forcing of Ticino and Toce catchments.

In both Toce and Ticino-Toce end moraine systems, terminal moraines of earlier glaciations are found external to the LGM position (Bini and Zuccoli, 2004; Montrasio et al., 1990; Piana et al., 2017). In the Verbano amphitheatre, pre-LGM glacier margins are cross-cut by LGM terminal moraines, e.g. around Gattico or Azzate (Fig. 5) where NW-SE respectively NE-SW running LGM terminal moraines cut through N–S oriented older ice-marginal deposits. Interestingly, no pre-LGM lateral moraines were identified along the sides of Orta and Verbano end moraine systems. Absence of preserved pre-LGM lateral ice margins in both lobes, suggests that previous glaciations, despite longer outrun, did reach similar lateral extents (ice surface heights) as they did during the last glaciation. That LGM moraines were deposited on top of ice-marginal deposits of previous glaciations in the Verbano end moraine system is independently confirmed by (a) a buried soil found within the Alpe Canà LGM maximum moraine and (b) pre-LGM erratics (VR30, VR44) buried by LGM ice margins and re-exhumed to the surface (section 4.1). The oldest erratic exposure age (101.9 ± 2.7 ka) thereby provides a minimum age for a previous foreland glaciation.

5.4. LGM on the southern side of the Alps

Within the last one and a half decades, the LGM glacier advances in many of the foreland reaching end moraine systems on the southern side of the Alps were successfully dated (this study; Bernoulli et al., 2018; Braakhekke et al., 2020; Federici et al., 2017; Gianotti et al., 2015; Ivy-Ochs et al., 2018; Monegato et al., 2017, 2007; Ravazzi et al., 2012a). Chronological data from other sites of the Southern Alps show good agreement with the LGM timing of the Ticino-Toce glacier (Fig. 1; Table 4). LGM maximum ages from Gesso Valley trunk glacier (24.0 ± 1.6 ka; Federici et al., 2017) and the Rivoli-Avigliana amphitheatre (24.0 ± 1.5 ka; Ivy-Ochs et al., 2018) overlap with those of the Ticino-Toce glacier within uncertainties. The maximum advance of the Como lobe, a part of the Adda glacier system, had to happen after 27.8–27.3 ka cal BP (Bernoulli et al., 2018; Castelletti et al., 2013). Oglio glacier system is chronologically defined within the inner Alpine Clusone amphitheatre. Dated to 26.4–25.3 ka cal BP (Ravazzi et al., 2012a) this advance shows good chronological concordance with the Ticino-Toce glacier. A synchronous LGM maximum is further reported

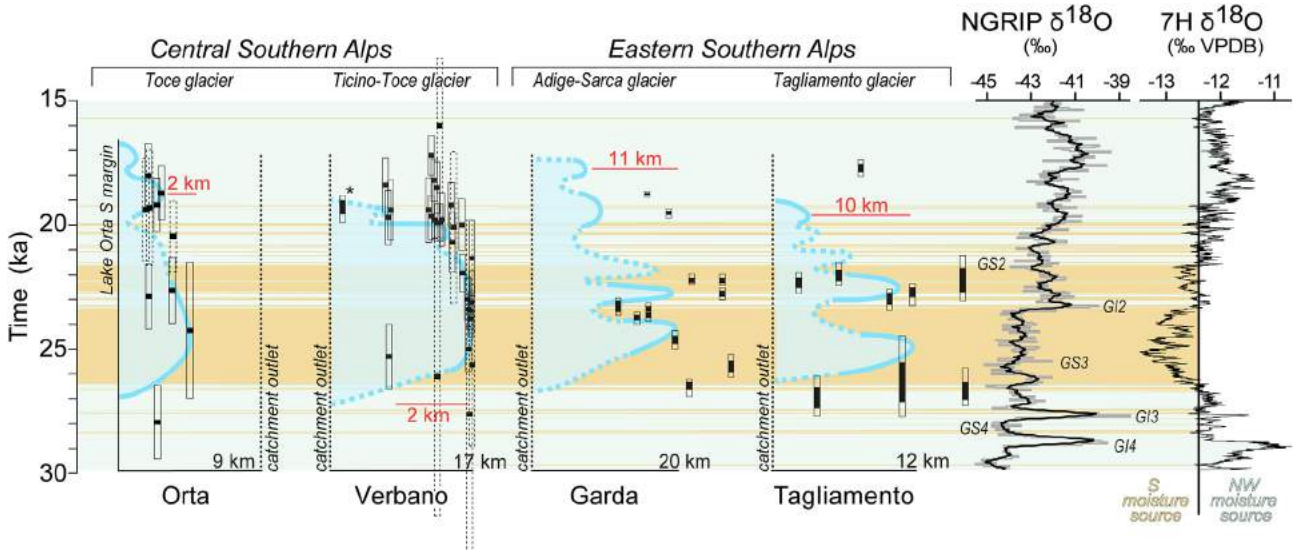

Fig. 13. Major LGM glacier oscillations of large piedmont glaciers in the central and eastern Southern Alps (Orta redrawn after Braakhekke et al., 2020; Verbano this study; Garda after Monegato et al., 2017; Tagliamento after Monegato et al., 2007) compared to the NGRIP $\delta^{18}O$ record (Svensson et al., 2006) and 7H $\delta^{18}O$ record from Sieben Hengste cave (Luetscher et al., 2015). Orta and Verbano are constrained with exposure ages (solid bar outline represents ^{10}Be ages, dashed bar outline shows ^{36}Cl ages). Minimum age for deglaciation of Verbano is given by a calibrated radiocarbon age from Lake Monate indicated by an asterisk (Rey et al., 2020). Garda and Tagliamento are constrained with calibrated radiocarbon ages (95.4% probability range is indicated with bar outline; black fill shows 68.2% probability range). Yellow and light green banners highlight phases of prevailing southerly and northwesterly moisture transport to the Alps, respectively (Luetscher et al., 2015). (For interpretation of the references to colour in this figure legend, the reader is referred to the Web version of this article.)

from the Adige-Sarca glacier in the Garda amphitheatre (25.0–24.2 ka cal BP; Monegato et al., 2017). The Tagliamento glacier in the NE of Italy reached its LGM maximum position on the foreland slightly earlier between 28.0 ka cal BP and 24.5 ka cal BP (Monegato et al., 2007). A bimodal LGM climax, with two separate glacier advances similar in size, as found in the Garda and Tagliamento amphitheatres (Monegato et al., 2007, 2017), is however not supported for the Verbano end moraine system (Fig. 13). Within the framework of uncertainties and the absence of other sedimentary evidence, a continuous LGM maximum of Ticino-Toce glacier between 25.0 ± 0.9 ka to 19.9 ± 0.7 ka with only minor glacier oscillations is suggested. The inner stadials of Verbano (19.7 ± 1.1 ka) and Orta lobes (19 ± 1 ka; Braakhekke et al., 2020), temporally coincide with a readvance stadial recorded in the Rivoli-Avigliana end moraine system dated to 19.6 ± 0.9 ka (Ivy-Ochs et al., 2018). Recessional positions between about 22–20 ka have further been reported for the Dora Baltea (Gianotti et al., 2015), Adda (Alessio et al., 1978; Bernoulli et al., 2018; Bini, 1997; Scapozza et al., 2014), and Piave glacier systems (Table 4; Carton et al., 2009). The final glacier collapse of the Adige-Sarca glacier and its withdrawal from the Garda basin occurred at about 17.8–17.2 ka cal BP (Ravazzi et al., 2014).

LGM chronologies that have been inferred directly from the ice margins of various glacier systems are in good agreement with available dates of downstream outwash sediments on the Italian plains. Sediment aggradation of alluvial (mega)fans along the southern Alpine fringe was shown to have peaked between 26 ka cal BP and 19 ka cal BP (26–21 ka cal BP for the Venetian-Friulian Plain (Fig. 1)) when glaciers resided close to their maximum extents (Fontana et al., 2014b). This build-up phase was followed by a drastic decrease in sediment delivery and by channel incision once deglaciation set in. By 19–17 ka cal BP, the newly formed intramorainic lakes acted as effective traps, cutting off sediment supply (Fontana et al., 2014b; Hinderer, 2001). Detailed studies on fan formation focused on the Venetian-Friulian Plain in NE Italy (Fontana et al., 2014a; Rossato et al., 2018; Rossato and Mozzi, 2016) and the outwash deposits of the Adda and Oglio glacier systems (Ravazzi et al., 2012b). Little data is available for the Italian piedmont plains to the west, among them the outwash sediments of the Ticino-Toce glacier system. Similar to many of the Italian amphitheatres (Balestro et al., 2009; Bini and Zuccoli, 2004; Carraro et al., 1975; Carraro and Petrucci, 1969; Feruglio, 1925, 1929; Petrucci, 1970; Sacco, 1927), the LGM extent of the Verbano lobe was underestimated in the past (Bini et al., 2014; Sacco, 1892). With increasing insights into LGM glacier behaviour it becomes more and more evident that the morphology in each of the Italian end moraine systems may be a product of a different number of glacier advances. In the end moraine systems in the western sector of the Southern Alps, including Verbano and Orta amphitheatres, LGM was less extensive compared to previous glaciation. On site, footprints of older Pleistocene glaciation are still preserved (Carraro et al., 1991; Fioraso et al., 2021; Gianotti et al., 2008, 2015; Ivy-Ochs et al., 2018; Ravazzi et al., 2012a). In contrast in the east, LGM glacier extents were comparably larger and overran previous ice-marginal deposits. The corresponding amphitheatres of Garda and Tagliamento were strongly reshaped during the ultimate glaciation and LGM ridges dominate the morphology of the end moraine systems (Monegato et al., 2007, 2017). The complex architecture of the Italian morainic amphitheatres underlines that chronological information is essential when the goal is to correlate ice margins across different end moraine systems.

5.5. LGM across the Alps: N–S to W-E perspective

LGM timing is unequally well constrained across the whole expanse of the Alps. Abundance and detail of available chronologies are generally better in the Western (Swiss) Alps and south of the Alpine divide. Except for the Rhone catchment (Graf et al., 2015; Ivy-Ochs, 2015; Ivy-Ochs et al., 2004a; Preusser et al., 2007; Rey et al., 2020), the chronological record of north Alpine glacier systems is fragmentary (Gaar et al., 2019). Robust chronologies covering the full LGM advance cycle are scarce due to rare availability of comprehensive sample material for cosmogenic (Akçar et al., 2011), or radiocarbon dating. Single LGM reference points (e.g. onset of glaciation, ice surface lowering, dated recessional stadials) are however available for most of the large glacier systems (Ivy-Ochs et al. (2022) provide an updated synthesis).

Available chronological information for the Swiss Alps, supports an in-phase LGM maximum of Alpine glaciers rather than a distinct time shift along a N–S gradient. The LGM of major glacier system in the northern Swiss Alps (Rhone, Aare, Reuss, and Rhein) temporally largely coincides with maximum stands of piedmont glaciers in the south. The Rhone LGM was dated to about 24 ± 2 ka with recessional positions at 22–20 ka (Ivy-Ochs, 2015; Ivy-Ochs et al., 2004a). A minimum age for the LGM maximum phase of the Aare glacier is provided by recessional phases near Bern dated to ca.

Table 4
Chronological constraints on LGM glacier timing in the Southern Alps.

	Major glacier systems	End moraine system/ amphitheatre	Method	LGM age constraints*		Reference
				Maximum	Readvance/recession	
West	Gesso (Gesso Valley)		^{10}Be	24.0 ± 1.6 ka		Federici et al. (2017)
	Dora Riparia (Susa Valley)	Rivoli-Avigliana	^{10}Be	24.0 ± 1.5 ka	19.6 ± 0.9 ka	Ivy-Ochs et al. (2018)
	Dora Baltea (Aosta Valley)	Ivrea	^{10}Be		20.1 ± 3.0 ka	Gianotti et al. (2015)
	Toce (Ossola Valley)	Orta	^{10}Be,^{36}Cl	26.5–23 ka	19 ± 1 ka	Braakhekke et al. (2020)
	Ticino-Toce (Ossola & Ticino Valley)	Verbano	^{10}Be,^{36}Cl	25.0 ± 0.9 ka	19.7 ± 1.1 ka	this study
	Adda (Valtellina)	Lario Lecco	^{14}C		22.4–21.7 ka cal BP	Alessio et al. (1978);
					21.7–20.6 ka cal BP	Bini (1997)
		Como	^{14}C	<27.8–27.3 ka cal BP		Castelletti et al. (2013); Bernoulli et al. (2018)
	Oglio (Camonica Valley)	Clusone Iseo	^{14}C	26.4–25.3 ka cal BP		Ravazzi et al. (2012a)
	Adige/Garda (Adige-Sarca Valley)	Garda	^{14}C	25.0–24.2 ka cal BP	23.3–23.1 ka cal BP	Monegato et al. (2017)
	Piave (Piave Valley)	Quero Vittorio Veneto	^{14}C		22.2–20.6 ka cal BP	Carton et al. (2009)
East	Tagliamento (Tagliamento Valley)	Tagliamento	^{14}C	28.0–24.5 ka cal BP	23.2–22.8 ka cal BP	Monegato et al. (2007)

*all ages calibrated using IntCal20 (Bronk Ramsey, 2009; Reimer et al., 2020) or recalculated using NENA (Balco et al., 2009) for more information see section 3.2.

21–19 ka (Akçar et al., 2011; Wüthrich et al., 2018). OSL ages from the Reuss glacier system show that the glacier must have reached its maximum position before 25.1 ± 2.4 ka and 24.4 ± 2.2 ka (Gaar et al., 2019). Two surface exposure ages in the range of 22 ± 1 ka further indicate enduring stabilization of LGM Reuss glacier on the foreland (Reber et al., 2014). Recent OSL and bone radiocarbon ages determined from outwash sediments in front of Rhein glacier terminal moraines support an early LGM around 26–25 ka (Preusser et al., 2007), in line with glaciers in the south.

An otherwise simultaneous glacier timing in the Western Alps compares to a distinctly earlier LGM glaciation of the southwestern Alpine foreland. The Lyon glacier lobe was recently found to have peaked twice with similar ice extent during 75–60 ka (MIS 4) and 40–30 ka (late MIS 3), respectively (Gribenski et al., 2021). The latter glacier maximum, predates LGM advances from northern, southern, and eastern Alpine forelands (Monegato et al., 2017).

For the northeastern parts of the Alps, chronological data on LGM culmination exists for two of the big paleoglacier systems (Fig. 1). Erratic boulder exposure ages from the Isar-Loisach outlet glacier, from the Bavarian foreland, range between 20 ka and 14 ka (Reuther et al., 2011). The wide spread and the comparably young ages either indicate long-lasting moraine stabilization (Reuther et al., 2011) or point to profound human impact. At Salzach glacier, a second LGM advance was luminescence dated to around 21–20 ka (Starnberger et al., 2011) and chronologically overlaps with readvance or recessional stadials reported in other glacier systems to the south and west (this study; Alessio et al., 1978; Bini, 1997; Braakhekke et al., 2020; Carton et al., 2009; Gianotti et al., 2015; Graf et al., 2015; Ivy-Ochs et al., 2018, 2004a; Jorda et al., 2000; Wüthrich et al., 2018).

Inner Alpine data suggest that ice surface lowering set in simultaneously across the Alps (18.6 ± 1.4 ka in the Tyrolian Alps (Wirsig et al., 2016a); 18.5 ± 1.1 ka in the Mont Blanc area (Wirsig et al., 2016a); 18 ± 1 ka in the central and southern Swiss Alps (Dielforder and Hetzel, 2014; Wirsig et al., 2016b)). Bedrock exposure ages from Montecrestese (Fig. 3) indicate that the Toce glacier had vanished from the valley bottom of Ossola Valley by 17.7 ± 0.9 ka to 16.1 ± 0.6 ka (Dielforder and Hetzel, 2014). The ice transfluences from the Rhone ice dome across Simplon Pass into the Toce catchment (Fig. 2a; Fig. 3) were estimated to have ceased around 18 ka with final deglaciation of the pass around 14.1 ± 0.4 ka (Dielforder and Hetzel, 2014). Similarly, surface exposure dates from Gotthard Pass (Fig. 3; Hippe et al., 2014) and radiocarbon ages from San Bernardino Pass and Lukmanier Pass (Fig. 3; Scapozza et al., 2014) point to ice free conditions in the high mountain areas of the Ticino catchment by 16–14 ka. Parallel to ice surface lowering in the High Alps, the deglaciation of the forelands was underway by 19–18 ka across the Alpine belt (Beckmann, 2004; Egger, 2007; Klasen et al., 2007; Lister, 1988; Ravazzi et al., 2012a, 2014; Reber et al., 2014; Rey et al., 2020; Schmidt et al., 1998; van Husen, 1977, 1987; van Husen et al., 2007). This was followed by the phase of Lateglacial ice decay, characterized by stagnant valley glaciers filling the main valleys and massive glacier downwasting (Reitner, 2007; van Husen, 1997).

5.6. New insights on LGM atmospheric circulation patterns in the Alps

During glacial times, Northern Hemisphere ice sheets exerted strong control on large-scale atmospheric and oceanic circulation (Beghin et al., 2015; Hofer et al., 2012a; Laîné et al., 2009; Löfverström et al., 2014). With ice surface heights between 3 and 4.5 km (Löfverström et al., 2016), the Laurentide ice sheet represented a large topographic obstacle (Roe and Lindzen, 2001) forcing the deflection of the Polar jet stream down to around 40°N (Hofer et al., 2012a, 2012b; Laîné et al., 2009; Löfverström et al., 2014; Pausata et al., 2011). The cooling of the northern North Atlantic and a more southern position of the sea ice margin also contributed to the Polar fronts southward migration (Hofer et al., 2012a). While overall circulation patterns have been reproduced by a number of atmospheric models (Hofer et al., 2012a, 2012b; Laîné et al., 2009; Löfverström et al., 2014; Pausata et al., 2011), details on intensity and position of the storm track and resulting major moisture delivery paths remain ambiguous (Višnjević et al., 2020). Analysis of different climate simulations points to an overall stronger storm track activity and associated high precipitation over southwestern Europe during the LGM (Ludwig et al., 2016). Based on paleo-equilibrium line altitudes and sea surface temperatures, Kuhlemann et al. (2008) reconstruct enhanced LGM precipitation rates along storm tracks located just east of the Gulf of Genoa, including the Southern Alps (Višnjević et al., 2020), attributed to increased cyclonic frequency in the gulf itself. Numerical ice flow simulations likewise support a predominant southwesterly moisture transport with simultaneous precipitation reduction in the Northern Alps (Becker et al., 2016). Detailed regional precipitation patterns derived from an Alpine speleothem record (Sieben Hengste (7H) cave, Swiss Alps; Fig. 1) indicate preferential moisture advection from the south between 26.5 ka and 23 ka that only after 23 ka changed in favour of a NW trajectory (Fig. 13; Luetscher et al., 2015). Meridional advection of warm, humid air towards the Alps may have been the dominant transport during the first half of the LGM (Luetscher et al., 2015). Such a pathway may be related to more frequent Rossby-wave breaking over Western Europe in the framework of a low latitude jet stream and the Eurasian ice sheet (Luetscher et al., 2015). Based on the age range of cryogenic carbonate formation in the Obir cave system (Fig. 1), Spötl et al. (2021) discuss enhanced autumn and early winter snowfall in the Austrian Karawanks from 26.6 ka to 23.5 ka, coinciding with southerly moisture advection (Luetscher et al., 2015).

Dominant western moisture transport and high precipitation rates in the southwestern Alpine massifs during progressive southward deflection of the polar storm track were recently proposed to have conditioned an early glacier maximum of the Lyon lobe at 40–30 ka (Gribenski et al., 2021). Moisture transport to this part of the Alps was likely reduced after 30 ka (preventing later glacier advances of comparable size) in line with the polar front approaching 40°N and the establishment of a predominantly southerly circulation (Gribenski et al., 2021). The suggested southern moisture advection during the LGM (Kuhlemann et al., 2008; Luetscher et al., 2015; Spötl et al., 2021) matches the locations of geomorphologically reconstructed Alpine ice domes that were for the most part at or just south of the principle weather divide (Florineth and Schlüchter, 2000; 1998). These crucial accumulation areas may have benefited from prevailing influx of meridional air masses during an early LGM (26.5–23 ka; Monegato et al., 2017). Ultimately, this may have conditioned an earlier regional glacier maximum on the southern side of the Alps (Monegato et al., 2017) close to 25.3 ka (Luetscher et al., 2015) and confirmed by the chronology of the Verbano end moraine system (Fig. 13). Non-uniform ice build-up and glacier advances across the Alps are supported by recent ice sheet modelling results (Seguinot et al., 2018) and apparent when comparing details of available glacier chronologies from the south (Fig. 13). LGM maximum stands of Garda and Tagliamento glaciers (Monegato et al., 2007, 2017), in the eastern part of the Southern Alps, coincide in the central-western sector with the arrival of the Toce-Ticino glacier at the maximum position (Braakhekke et al., 2020; this work). Their timing matches with an early phase of strong southerly air flow in the 7H record (Fig. 13; Luetscher et al., 2015; Monegato et al., 2017). With the progressive re-establishment of the westerlies, Garda and

Tagliamento glaciers remained inside their former LGM limits. Gradually cut-off from southerly moisture supply, the shift in precipitation likely did not allow the maintenance of their large outlet glaciers after ca. 22 ka (Fontana et al., 2014a; Monegato et al., 2017, Fig. 13). A similar behaviour, even if not strongly chronologically constrained, can be inferred for the Dora Baltea system at Ivrea (Fig. 1; Gianotti et al., 2015). Unlike glaciers in the eastern sector of the Southern Alps, no significant ice loss is observed in the end moraine systems of the central Southern Alps around that time. On the contrary, Orta and Verbano lobes remained remarkably close to their LGM maximum position over the time period 26.5–19 ka (Braakhekke et al., 2020) and 25.0 ± 0.9 ka to 19.9 ± 0.7 ka, respectively. In order to maintain its mass balance, precipitation delivery to the accumulation area of the Ticino-Toce glacier must have persisted beyond 23 ka. Ticino and Toce glacier systems may not have been as dependent on southerly moisture advection as glacier systems further to the east. Ice build-up in the study area may have profited from the intermediate position of the Ticino and Toce catchments, being in reach of both southerly air flow as well as westerly moisture advection. In light of differing insights from the sectors of the Southern Alps, the behaviour of the large outlet glaciers is particular interesting. Further chronological constraints on the (last) glaciation of the Southern Alps (and the overall mountain range) are considered key to deepen our understanding of regional LGM climate patterns.

6. Conclusions

Bridging latest chronological constraints from end moraine systems in the western and eastern parts of the Southern Alps, this study introduces new insights into LGM glacier advances in the central Southern Alps. By means of geomorphological analysis, sedimentological investigations, and extensive surface exposure dating a glacier chronology was established that reconstructs behaviour of the Ticino-Toce glacier at the peak of the last glaciation in detail.

We define the LGM of the Ticino-Toce glacier as a 5000-year time period lasting from 25.0 ± 0.9 ka to 19.9 ± 0.7 ka, during which the glacier front fluctuated relatively close to its maximum position. Formation of multiple lateral ice margins falls into this time period, indicating a sustained glacier front in balance with ice supply from the catchment. Contrary to the most recent interpretation (Bini et al., 2009), the LGM Ticino-Toce glacier did advance several kilometres further south, thereby filling the basins of, and between, Lake Maggiore and Lake Varese completely. The highest lateral moraines on both sides of the end moraine system were, without exception, dated to the LGM. That earlier glaciations reached ice surface heights comparable to the last glaciation is further indicated by scattered erratics with ages up to 101.9 ± 2.7 ka. Five boulders had pre-LGM ages, that we interpret to be minimum ages. Pre-LGM moraines on the right side of the Verbano end moraine system were apparently re-occupied during the LGM. At the glacier front, three moraine sets could be assigned to the LGM. The multi-ridged external ice margin is characterized by distinct morphology and only weak signs of weathering of the sediment. These frontal moraines further connect to LGM dated lateral moraines and are independently constrained by two ^{36}Cl exposure ages. Internal to those, an intermediate frontal moraine can be connected to chronologically well-constrained lateral deposits based on geomorphology or altitudinal relationships. Located two kilometres internal to the LGM maximum moraines, the innermost ice margin probably correlates to a short-lived glacier readvance identified based on sedimentological evidence. This readvance occurred around 19.7 ± 1.1 ka, most likely followed by the final deglaciation of the foreland.

Timing of the Ticino-Toce glacier is in good agreement with available chronological constraints from other amphitheatres in the south and the major Swiss glacier systems (Rhone, Aare, Reuss, and Rhein). Taken together, the evidence points to synchronous maximum advance in this part of the Alps. Pronounced differences in glacier regime were however discovered between glacier systems in the central and eastern Southern Alps. While for the latter, glacier front fluctuations in the order of several kilometres were reported (Monegato et al., 2007, 2017), Orta (Braakhekke et al., 2020) and Verbano piedmont lobes likely remained close to their LGM maximum positions over several millennia. Stable ice masses reconstructed for the central Southern Alps may point to a smaller dependency on meridional moisture transport compared to glaciers in the east. This unexpected insight underlines the value of and need for comprehensive glacier chronologies combined with extensive geomorphological fieldwork for the reconstruction of paleoclimate at the regional scale.

Author contributions

All authors provided substantial contributions to the submitted worked. SIO conceptualized the work together with GM and FG. Funding was acquired by SIO with help of GM. Implementation of the project was under supervision of SIO and GM. Project resources and administration were covered by SIO and HAS. Field investigations were undertaken by SK, SIO, GM, and FG. SK, SIO, CV, MC, and NA were in charge of methodological aspects and data curation. Data analysis and visualization in ArcGIS and Illustrator software was performed by SK. The original draft of the manuscript was written by SK, SIO, and GM. All authors were involved in the revision of the text and have approved the final version of the manuscript.

Declaration of competing interest

The authors declare that they have no known competing financial interests or personal relationships that could have appeared to influence the work reported in this paper.

Acknowledgements

Sincere thanks go to Olivia Steinemann and Ewelina Broś for their guidance through sample preparation. We thank Andrea Zamboni and his team for their expertise in interpreting the soil pits. All members of the Ion Beam Physics group at ETH Zurich are thanked for their contributions to the excellent AMS results. We appreciate the consent of Campo dei Fiori Regional Park, Parco Naturale Valle Ticino, and the municipality of Gattico-Veruno for authorizing sampling of protected erratic boulders. Careful and insightful reviews by Cristian Scapozza and Jakob Heyman considerably improved the manuscript. Funding by the Swiss National Science Foundation is gratefully acknowledged [SNF grant number 175794, 2017].

References

Akçar, N., Ivy-Ochs, S., Kubik, P.W., Schlüchter, C., 2011. Post-depositional impacts on "Findlinge" (erratic boulders) and their implications for surface-exposure dating. Swiss J. Geosci. 104, 445–453.

Alessio, M., Allegri, L., Bella, F., Belluomini, G., Calderoni, G., Cortesi, C., Improta, S., Manfra, L., Orombelli, G., 1978. I depositi lacustri di Rovagnate, di Pontida e di Pianico in Lombardia: datazione 14C. Geogr. Fis. Din. Quaternaria 1, 131–137.

Alfimov, V., Ivy-Ochs, S., 2009. How well do we understand production of 36Cl in limestone and dolomite? Quat. Geochronol. 4, 462–474.

André, M., 2002. Rates of postglacial rock weathering on glacially scoured outcrops

(abisko–riksgränsen area, 68° n). Geogr. Ann. Ser. A. Phys. Geogr. 84, 139–150.
Balco, G., Briner, J., Finkel, R.C., Rayburn, J.A., Ridge, J.C., Schaefer, J.M., 2009. Regional beryllium-10 production rate calibration for late-glacial northeastern North America. Quat. Geochronol. 4, 93–107.
Balco, G., Stone, J.O., Lifton, N.A., Dunai, T.J., 2008. A complete and easily accessible means of calculating surface exposure ages or erosion rates from 10Be and 26Al measurements. Quat. Geochronol. 3, 174–195.
Balestro, G., Spagnolo, G., Lucchesi, S., Fioraso, G., Forno, M.G., Cadoppi, P., Tallone, S., Piccardo, G.B., Polino, R., 2009. Carta Geologica d'Italia alla scala 1: 50.000. Foglio 155 Torino Ovest. ISPRA – Istituto Superiore per la Protezione e la Ricerca Ambientale.
Becker, P., Seguinot, J., Jouvet, G., Funk, M., 2016. Last Glacial Maximum precipitation pattern in the Alps inferred from glacier modelling. Geograph. Helv. 71, 173–187.
Beckmann, M., 2004. Pollenanalytische Untersuchung der Zeit der Jäger und Sammler und der ersten Bauern an zwei Lokalitäten des Zentralen Schweizer Mittellandes Umwelt und erste Eingriffe des Menschen in die Vegetation vom Paläolithikum bis zum Jungneolithikum. Dissertationes botanicae Bd 390.
Beghin, P., Charbit, S., Dumas, C., Kageyama, M., Ritz, C., 2015. How might the North American ice sheet influence the northwestern Eurasian climate? Clim. Past. 11, 1467–1490.
Bernoulli, D., Ambrosi, C., Scapozza, C., Stockar, R., Schenker, F.L., Gaggero, L., Antognini, M., Bronzini, S., 2018. Foglio 1373 Mendrisio (parte Est) con parte Ovest del foglio Como. Atlante geologico della Svizzera, 1:25 000, Note esplicative 152. Bundesamt für Landestopografie swisstopo, Wabern.
Bini, A., 2012. I ghiacciai del Passato. In: Bonardi, L., Rovelli, E., Scotti, R., Toffaletti, A., Urso, M., Villa, F., Di Lombardia, I Ghiacciai (Eds.), Evoluzione e Attualità. Servizio Glaciologico Lombardo, Milano, pp. 11–19.
Bini, A., 1997. Stratigraphy, chronology and paleogeography of Quaternary deposits of the area between the Ticino and Olona rivers (Italy-Switzerland). Geol. Insubrica 2, 21–46.
Bini, A., Cita, M.B., Gaetani, M., 1978. Southern Alpine lakes - hypothesis of an erosional origin related to the Messinian entrenchment. Mar. Geol. 27, 271–288.
Bini, A., Schlüchter, C., Burkhalter, R.M., Urech, M., 2009. Die Schweiz während des letzteiszeitlichen Maximums (LGM). Bundesamt für Landestopografie swisstopo, Wabern.
Bini, A., Sciunnach, D., Bersezio, R., Scardia, G., Tomasi, F., 2014. Note illustrative della Carta geologica d'Italia alla scala, 1:50.000. Foglio 096 Seregno. ISPRA – Istituto Superiore per la Protezione e la Ricerca Ambientale.
Bini, A., Zuccoli, L., 2004. Glacial history of the southern side of the central Alps. Italy. Dev. Quat. Sci. 2, 195–200.
Borchers, B., Marrero, S., Balco, G., Caffee, M., Goehring, B., Lifton, N., Nishiizumi, K., Phillips, F., Schaefer, J., Stone, J., 2016. Geological calibration of spallation production rates in the CRONUS-Earth project. Quat. Geochronol. 31, 188–198.
Boriani, A., Burlini, L. (Eds.), 1995. Carta geologica della Valle Cannobina = Geological map of Valle Cannobina. Dipartimento di Scienze della Terra dell'Università degli Studi di Milano (Milano).
Braakhekke, J., Ivy-Ochs, S., Monegato, G., Gianotti, F., Martin, S., Casale, S., Christl, M., 2020. Timing and flow pattern of the Orta glacier (European Alps) during the last glacial maximum. Boreas 49, 315–332.
Brack, P., Ulmer, P., 2010. A crustal-scale magmatic system from the Earth's mantle to the Permian surface - field trip to the area of lower Valsesia and Val d'Ossola (Massiccio dei Laghi, Southern Alps, Northern Italy). Bull. für Angew. Geol. 15, 3–21.
Briner, J.P., Kaufman, D.S., Manley, W.F., Finkel, R.C., Caffee, M.W., 2005. Cosmogenic exposure dating of late Pleistocene moraine stabilization in Alaska. GSA Bull. 117, 1108–1120.
Bronk Ramsey, C., 2009. Bayesian analysis of radiocarbon dates. Radiocarbon 51, 337–360.
Carraro, F., Lanza, R., Perotto, A., Zanella, E., 1991. L'evoluzione morfologica del Biellese occidentale durante il Pliestocene inferiore e medio, in relazione all'inizio della costruzione dell'Anfiteatro Morenico d'Ivrea. Boll./Mus. Reg. di Sci. Nat. Torino 9, 99–117.
Carraro, F., Medioli, F., Petrucci, F., 1975. Geomorphological study of the morainic amphitheatre of Ivrea, Northwest Italy. R. Soc. N. Z. Bull. 13, 89–93.
Carraro, F., Petrucci, F., 1969. Carte Géologique de la Plaine du Piémont 1:400.000. VIII Congrés INQUA, Paris.
Carton, A., Bondesan, A., Fontana, A., Meneghel, M., Miola, A., Mozzi, P., Primon, S., Surian, N., 2009. Geomorphological evolution and sediment transfer in the Piave river system (northeastern Italy) since the last glacial maximum. Géomorphol. Relief, Process. Environ. 15, 155–174.
Castelletti, L., Livio, F., Martinelli, E., Michetti, A.M., Motella De Carlo, S., 2013. Recenti ricerche paleoecologiche in ambito lariano svolte in collaborazionefra Università dell'Insubria e Laboratorio di archeobiologia dei Musei Civici di Como. Riv. archeol. dell'antica Prov. e Diocesi di Como 195, 115–128.
Castiglioni, B., 1940. L'Italia nell'età quaternaria. Plate No. 3. In: Atlante Fisico-Economico d' Italia. Consociazione Turistica Italiana, Milano.
Cazzini, F.F., Amadori, C., Bosino, A., Fantoni, R., 2020. New seismic evidence of the Messinian paleomorphology beneath Lake Maggiore area (Italy). Ital. J. Geosci. 139, 195–211.
Chaline, J., Jerz, H., 1984. Arbeitsergebnisse der Subkommission für Europäische Quartärstratigraphie. Stratotypen des Würm-Glazials. Eiszeitalt. Ggw. 35, 185–206.
Christl, M., Vockenhuber, C., Kubik, P.W., Wacker, L., Lachner, J., Alfimov, V., Synal, H.A., 2013. The ETH Zurich AMS facilities: performance parameters and reference materials. Nucl. Instruments methods phys. Res. Sect. B Beam interact. With mater. Atoms 294, 29–38.
Claude, A., Ivy-Ochs, S., Kober, F., Antognini, M., Salcher, B., Kubik, P.W., 2014. The Chironico landslide (Valle Leventina, southern Swiss Alps): age and evolution. Swiss J. Geosci. 107, 273–291.
Dal Piaz, G.V., 2010. The Italian Alps: a journey across two centuries of Alpine geology. In: Beltrando, M., Peccerillo, A., Mattei, M., Conticelli, S., Doglioni, C. (Eds.), The Geology of Italy: Tectonics and Life along Plate Margins.
de Mortillet, G., 1861. Carte des anciens glaciers du versant Italien des Alpes. Atti della Soc. Ital. di Sci. Nat 3, 44–81.
Dielforder, A., Hetzel, R., 2014. The deglaciation history of the Simplon region (southern Swiss Alps) constrained by 10Be exposure dating of ice-molded bedrock surfaces. Quat. Sci. Rev. 84, 26–38.
Egger, H., 2007. Erläuterungen zur Geologischen Karte der Republik Österreich 1: 50.000. Blatt 67 Grünau i. Almtal. Geologische Bundesanstalt, Wien.
Ehlers, J., Gibbard, P.L., 2004. Quaternary glaciations - extent and chronology. Part I: Europe. Dev. Quat. Sci. 2 (Elsevier, Boston).
Ehlers, J., Gibbard, P.L., Hughes, P.D., 2011. Quaternary Glaciations - Extent and Chronology. A Closer Look. Elsevier, Amsterdam.
Evans, D., 2007. Glacitectonic structures and landforms. In: Encyclopedia of Quaternary Science, pp. 831–838.
Evans, J.M., Stone, J.O.H., Fifield, L.K., Cresswell, R.G., 1997. Cosmogenic chlorine-36 production in K-feldspar. Nucl. Instruments methods phys. Res. Sect. B Beam interact. With mater. Atoms 123, 334–340.
Federal Office of Meteorology and Climatology MeteoSwiss, 2016. Data portal IDAweb. URL. https://www.meteoswiss.admin.ch/home/services-and-publications/beratung-und-service/datenportal-fuer-experten.html.
Federal Office of Topography swisstopo, 2005. Geological Map of Switzerland 1: 500,000. Bundesamt für Landestopografie swisstopo, Wabern.
Federici, P.R., Ribolini, A., Spagnolo, M., 2017. Glacial history of the maritime Alps from the last glacial maximum to the little ice age. Geol. Soc. Spec. Publ. 433, 137–159.
Feruglio, E., 1929. Nuove ricerche sul Quaternario del Friuli. G. Geol. (Bologna) 2, 1–36.
Feruglio, E., 1925. Carta geologica delle Tre Venezie. Foglio 25 Udine. Ufficio Idrografico Regio Magistrato Acque di Venezia (Firenze).
Finckh, P., 1978. Are southern Alpine lakes former Messinian canyons? - geophysical evidence for preglacial erosion in the southern Alpine lakes. Mar. Geol. 27, 289–302.
Finckh, P., Kelts, K., Lambert, A., 1984. Seismic stratigraphy and bedrock forms in perialpine lakes. Geol. Soc. Am. Bull. 95, 1118–1128.
Fink, D., Vogt, S., Hotchkis, M., 2000. Cross-sections for 36Cl from Ti at Ep = 35-150 MeV: applications to in-situ exposure dating. Nucl. Instruments methods phys. Res. Sect. B Beam interact. With mater. Atoms 172, 861–866.
Fioraso, G., Monegato, G., Balestro, G., Hajdas, I., Baggio, P., 2021. Disentangling the stratigraphic architecture of the Rivoli-Avigliana end moraine system (Western Alps, NW Italy). J. Maps 17, 325–336.
Florineth, D., Schlüchter, C., 2000. Alpine evidence for atmospheric circulation patterns in Europe during the last glacial maximum. Quat. Res. 54, 295–308.
Florineth, D., Schlüchter, C., 1998. Reconstructing the last glacial maximum (LGM) ice surface geometry and flowlines in the central Swiss Alps. Eclogae Geol. Helv. 91, 391–407.
Fontana, A., Monegato, G., Zavagno, E., Devoto, S., Burla, I., Cucchi, F., 2014a. Evolution of an Alpine fluvioglacial system at the LGM decay: the Cormor megafan (NE Italy). Geomorphology 204, 136–153.
Fontana, A., Mozzi, P., Marchetti, M., 2014b. Alluvial fans and megafans along the southern side of the Alps. Sediment. Geol. 301, 150–171.
Frey, M., Desmons, J., Neubauer, F., 1999. The new metamorphic map of the Alps, Schweizerische mineralogische und petrographische Mitteilungen (Stäubli, Zürich).
Gaar, D., Graf, H.R., Preusser, F., 2019. New chronological constraints on the timing of Late Pleistocene glacier advances in northern Switzerland. Quat. Sci. J. 68, 53–73.
Gianola, O., Schmidt, M.W., von Quadt, A., Peytcheva, I., Luraschi, P., Reusser, E., 2014. Continuity in geochemistry and time of the tertiary Bergell intrusion (central Alps). Swiss J. Geosci. 107, 197–222.
Gianotti, F., Forno, M.G., Ivy-Ochs, S., Kubik, P.W., 2008. New chronological and stratigraphical data on the Ivrea amphitheatre (Piedmont, NW Italy). Quat. Int. 190, 123–135.
Gianotti, F., Forno, M.G., Ivy-Ochs, S., Monegato, G., Pini, R., Ravazzi, C., 2015. Stratigraphy of the Ivrea morainic amphitheatre (NW Italy): an updated synthesis. Alp. Mediterr. Quat. 28, 29–58.
Graf, A., Akçar, N., Ivy-Ochs, S., Strasky, S., Kubik, P.W., Christl, M., Burkhard, M., Wieler, R., Schlüchter, C., 2015. Multiple advances of Alpine glaciers into the Jura mountains in the northwestern Switzerland. Swiss J. Geosci. 108, 225–238.
Gribenski, N., Valla, P.G., Preusser, F., Roattino, T., Crouzet, C., Buoncristiani, J.-F., 2021. Out-of-phase Late Pleistocene glacial maxima in the Western Alps reflect past changes in North Atlantic atmospheric circulation. Geology.
Hantke, R., 1983. Eiszeitalter die jüngste Erdgeschichte der Schweiz und ihrer Nachbargebiete. Westliche Ostalpen mit ihrem bayerischen Vorland bis zum Inn-Durchbruch und Südalpen zwischen Dolomiten und Mont Blanc, third ed. (Ott Verlag, Thun).
Heyman, J., Applegate, P.J., Blomdin, R., Gribenski, N., Harbor, J.M., Stroeven, A.P., 2016. Boulder height - exposure age relationships from a global glacial 10Be compilation. Quat. Geochronol. 34, 1–11.

Heyman, J., Stroeven, A.P., Harbor, J.M., Caffee, M.W., 2011. Too young or too old: evaluating cosmogenic exposure dating based on an analysis of compiled boulder exposure ages. Earth Planet Sci. Lett. 302, 71–80.
Hinderer, M., 2001. Late Quaternary denudation of the Alps, valley and lake fillings and modern river loads. Geodin. Acta 14, 231–263.
Hippe, K., Ivy-Ochs, S., Kober, F., Zasadni, J., Wieler, R., Wacker, L., Kubik, P.W., Schlüchter, C., 2014. Chronology of Lateglacial ice flow reorganization and deglaciation in the Gotthard Pass area, Central Swiss Alps, based on cosmogenic 10Be and in situ 14C. Quat. Geochronol. 19, 14–26.
Hofer, D., Raible, C.C., Dehnert, A., Kuhlemann, J., 2012a. The impact of different glacial boundary conditions on atmospheric dynamics and precipitation in the North Atlantic region. Clim. Past 8, 935–949.
Hofer, D., Raible, C.C., Merz, N., Dehnert, A., Kuhlemann, J., 2012b. Simulated winter circulation types in the North Atlantic and European region for preindustrial and glacial conditions. Geophys. Res. Lett. 39, 2–6.
Ivy-Ochs, S., 2015. Glacier variations in the European Alps at the end of the last glaciation. Cuadernos Invest. Geogr. 41, 295–315.
Ivy-Ochs, S., 1996. The Dating of Rock Surfaces Using in Situ Produced 10Be, 26Al and 36Cl, with Examples from Antarctica and the Swiss Alps (dissertation). ETH Zürich, Zürich.
Ivy-Ochs, S., Kerschner, H., Reuther, A., Preusser, F., Heine, K., Maisch, M., Kubik, P.W., Schlüchter, C., 2008. Chronology of the last glacial cycle in the European Alps. J. Quat. Sci. 23, 559–573.
Ivy-Ochs, S., Kober, F., 2008. Surface exposure dating with cosmogenic nuclides. Quat. Sci. J. 57, 179–209.
Ivy-Ochs, S., Lucchesi, S., Baggio, P., Fioraso, G., Gianotti, F., Monegato, G., Graf, A., Akçar, N., Christl, M., Carraro, F., Forno, M.G., Schlüchter, C., 2018. New geomorphological and chronological constraints for glacial deposits in the Rivoli-Avigliana end-moraine system and the lower Susa Valley (Western Alps, NW Italy). J. Quat. Sci. 33, 550–562.
Ivy-Ochs, S., Monegato, G., Reitner, J.M., 2022. The Alps: glacial landforms from the last glacial maximum. In: Palacios, D., Hughes, P.D., Ruiz, J.M.G., de Andrés, N. (Eds.), European Glacial Landscapes: Maximum Extent of Glaciations. Elsevier, Amsterdam, pp. 449–460.
Ivy-Ochs, S., Schäfer, J., Kubik, P.W., Synal, H.A., Schlüchter, C., 2004a. Timing of deglaciation on the northern Alpine foreland (Switzerland). Eclogae Geol. Helv. 97, 47–55.
Ivy-Ochs, S., Synal, H.-A., Roth, C., Schaller, M., 2004b. Initial results from isotope dilution for Cl and 36Cl measurements at the PSI/ETH Zurich AMS facility. Nucl. Instrum. Methods Phys. Res. B 223–224, 623–627.
Jäckli, H., Hantke, R., Imhof, E., Leuzinger, H., 1970. Die Schweiz zur letzten Eiszeit = La Suisse durant la dernière période glaciaire = La Svizzera durante l'ultima glaciazione. Atlas der Schweiz 6. Eidg. Landestopographie, Wabern.
Jorda, M., Rosique, T., Évin, J., 2000. Donnees nouvelles sur l'age du dernier maximum glaciaire dans les Alpes meridionales francaises. Comptes Rendus l'Academie Sci. Ser. IIa Sci.. la Terre des Planetes 331, 187–193.
Kelly, M.A., Buoncristiani, J.F., Schlüchter, C., 2004. A reconstruction of the last glacial maximum (LGM) ice-surface geometry in the western Swiss Alps and contiguous Alpine regions in Italy and France. Eclogae Geol. Helv. 97, 57–75.
Klasen, N., Fiebig, M., Preusser, F., Reitner, J.M., Radtke, U., 2007. Luminescence dating of proglacial sediments from the Eastern Alps. Quat. Int. 164–165, 21–32.
Kohl, C.P., Nishiizumi, K., 1992. Chemical isolation of quartz for measurement of in-situ-produced cosmogenic nuclides. Geochem. Cosmochim. Acta 56, 3583–3587.
Kronig, O., Ivy-Ochs, S., Hajdas, I., Christl, M., Wirsig, C., Schlüchter, C., 2018. Holocene evolution of the Triftje- and the Oberseegletscher (Swiss Alps) constrained with 10Be exposure and radiocarbon dating. Swiss J. Geosci. 111, 117–131.
Kuhlemann, J., Rohling, E.J., Krumrei, I., Kubik, P., Ivy-Ochs, S., Kucera, M., 2008. Regional synthesis of mediterranean atmospheric circulation during the last glacial maximum. Science 321, 1338–1340.
Laîné, A., Kageyama, M., Salas-Mélia, D., Voldoire, A., Rivièlre, G., Ramstein, G., Planton, S., Tyteca, S., Peterschmitt, J.Y., 2009. Northern hemisphere storm tracks during the last glacial maximum in the PMIP2 ocean-atmosphere coupled models: energetic study, seasonal cycle, precipitation. Clim. Dynam. 32, 593–614.
Lal, D., 1991. Cosmic ray labeling of erosion surfaces: in situ nuclide production rates and erosion models. Earth Planet Sci. Lett. 104, 424–439.
Larocque, I., Finsinger, W., 2008. Late-glacial chironomid-based temperature reconstructions for Lago Piccolo di Avigliana in the southwestern Alps (Italy). Palaeogeogr. Palaeoclimatol. Palaeoecol. 257, 207–223.
Lister, G.S., 1988. A 15,000-year isotopic record from Lake Zürich of deglaciation and climatic change in Switzerland. Quat. Res. 29, 129–141.
Löfverström, M., Caballero, R., Nilsson, J., Kleman, J., 2014. Evolution of the large-scale atmospheric circulation in response to changing ice sheets over the last glacial cycle. Clim. Past 10, 1453–1471.
Löfverström, M., Caballero, R., Nilsson, J., Messori, G., 2016. Stationary wave reflection as a mechanism for zonalizing the atlantic winter jet at the LGM. J. Atmos. Sci. 73, 3329–3342.
Ludwig, P., Schaffernicht, E.J., Shao, Y., Pinto, J.G., 2016. Regional atmospheric circulation over Europe during the last glacial maximum and its links to precipitation. J. Geophys. Res. Atmos. 121, 2130–2145.
Luetscher, M., Boch, R., Sodemann, H., Spötl, C., Cheng, H., Edwards, R.L., Frisia, S., Hof, F., Müller, W., 2015. North Atlantic storm track changes during the last glacial maximum recorded by Alpine speleothems. Nat. Commun. 6, 27–32.
Marrero, S.M., Phillips, F.M., Caffee, M.W., Gosse, J.C., 2016. CRONUS-Earth cosmogenic 36Cl calibration. Quat. Geochronol. 31, 199–219.
Mattirolo, E., Novarese, V., Taricco, M., Pullè, G., Fossa Mancini, E., Catalisano, S., 1932. Carta Geologica d'Italia alla scala 1: 100,000. Foglio 31 Varese. Real Ufficio Geologico, Stabilimenti L. Salomone, Roma.
Monegato, G., Ravazzi, C., Donegana, M., Pini, R., Calderoni, G., Wick, L., 2007. Evidence of a two-fold glacial advance during the last glacial maximum in the Tagliamento end moraine system (Eastern Alps). Quat. Res. 68, 284–302.
Monegato, G., Scardia, G., Hajdas, I., Rizzini, F., Piccin, A., 2017. The Alpine LGM in the boreal ice-sheets game. Sci. Rep. 7, 1–8.
Montrasio, A., Bigioggero, B., Maino, A., Cirese, E., Tacchiao, D., 1990. Carta Geologica Della Lombardia: Scala, vol. 1, 250.000. Servizio Geologico Nazionale, Roma.
Oberhänsli, R., Bousquet, R., Engi, M., Goffé, B., Gosso, G., Handy, M., Häck, V., Koller, F., Lardeaux, J.M., Polino, R., Rossi, P., Schuster, R., Schwartz, S., Spalla, M.I., 2004. Metamorphic Structure of the Alps. CCGM/CGMV, Paris.
Omboni, G., 1861. I ghiacciai antichi e il terreno erratico di Lombardia. Atti della Soc. Ital. di Sci. Nat 3, 232–299.
Pausata, F.S.R., Li, C., Wettstein, J.J., Kageyama, M., Nisancioglu, K.H., 2011. The key role of topography in altering North Atlantic atmospheric circulation during the last glacial period. Clim. Past 7, 1089–1101.
Penck, A., Brückner, E., 1909. Die Alpen im Eiszeitalter. Tauchnitz, Leipzig. Chr. Herm.
Petrucci, F., 1970. Rilevamento geomorfologico dell'Anfiteatro morenico di Rivoli-Avigliana. Mem. Soc. Ital. Sci. Nat. 18, 95–124.
Piana, F., Fioraso, G., Irace, A., Mosca, P., D'Atri, A., Barale, L., Falletti, P., Monegato, G., Morelli, M., Tallone, S., Vigna, G.B., 2017. Geology of Piemonte region (NW Italy, Alps-Apennines interference zone). J. Maps 13, 395–405.
Preusser, F., Blei, A., Graf, H., Schlüchter, C., 2007. Luminescence dating of Würmian (Weichselian) proglacial sediments from Switzerland: methodological aspects and stratigraphical conclusions. Boreas 36, 130–142.
Preusser, F., Reitner, J.M., Schlüchter, C., 2010. Distribution, geometry, age and origin of overdeepened valleys and basins in the Alps and their foreland. Swiss J. Geosci. 103, 407–426.
Putkonen, J., Swanson, T., 2003. Accuracy of cosmogenic ages for moraines. Quat. Res. 59, 255–261.
Ravazzi, C., Badino, F., Marsetti, D., Patera, G., Reimer, P.J., 2012a. Glacial to paraglacial history and forest recovery in the Oglio glacier system (Italian Alps) between 26 and 15 ka cal BP. Quat. Sci. Rev. 58, 146–161.
Ravazzi, C., Deaddis, M., Amicis, M., De Marchetti, M., Vezzoli, G., Zanchi, A., 2012b. The last 40 ka evolution of the Central Po Plain between the Adda and Serio rivers. Geomorphol. Reli. Process. Environ. 18, 131–154.
Ravazzi, C., Pini, R., Badino, F., De Amicis, M., Londeix, L., Reimer, P.J., 2014. The latest LGM culmination of the Garda Glacier (Italian Alps) and the onset of glacial termination. Age of glacial collapse and vegetation chronosequence. Quat. Sci. Rev. 105, 26–47.
Reber, R., Akçar, N., Ivy-Ochs, S., Tikhomirov, D., Burkhalter, R., Zahno, C., Lüthold, A., Kubik, P.W., Vockenhuber, C., Schlüchter, C., 2014. Timing of retreat of the Reuss glacier (Switzerland) at the end of the last glacial maximum. Swiss J. Geosci. 107, 293–307.
Reimer, P.J., Austin, W.E.N., Bard, E., Bayliss, A., Blackwell, P.G., Bronk Ramsey, C., Butzin, M., Cheng, H., Edwards, R.L., Friedrich, M., Grootes, P.M., Guilderson, T.P., Hajdas, I., Heaton, T.J., Hogg, A.G., Hughen, K.A., Kromer, B., Manning, S.W., Muscheler, R., Palmer, J.G., Pearson, C., van der Plicht, J., Reimer, R.W., Richards, D.A., Scott, E.M., Southon, J.R., Turney, C.S.M., Wacker, L., Adolphi, F., Büntgen, U., Capano, M., Fahrni, S.M., Fogtmann-Schulz, A., Friedrich, R., Köhler, P., Kudsk, S., Miyake, F., Olsen, J., Reinig, F., Sakamoto, M., Sookdeo, A., Talamo, S., 2020. The IntCal20 northern hemisphere radiocarbon age calibration curve (0–55 cal kBP). Radiocarbon 62, 725–757.
Reitner, J.M., 2007. Glacial dynamics at the beginning of Termination I in the Eastern Alps and their stratigraphic implications. Quat. Int. 164–165, 64–84.
Reuther, A.U., Fiebig, M., Ivy-Ochs, S., Kubik, P.W., Reitner, J.M., Jerz, H., Heine, K., 2011. Deglaciation of a large piedmont lobe glacier in comparison with a small mountain glacier – new insight from surface exposure dating. Two studies from SE Germany. Quat. Sci. J. 60, 248–269.
Rey, F., Gobet, E., Schwörer, C., Hafner, A., Szidat, S., Tinner, W., 2020. Climate impacts on vegetation and fire dynamics since the last deglaciation at Moossee (Switzerland). Clim. Past 16, 1347–1367.
Roe, G., Lindzen, R., 2001. The mutual interaction between continental-scale ice sheets and atmospheric stationary waves. J. Clim. 14, 1450–1465.
Rossato, S., Carraro, A., Monegato, G., Mozzi, P., Tateo, F., 2018. Glacial dynamics in pre-Alpine narrow valleys during the Last Glacial Maximum inferred by lowland fluvial records (northeast Italy). Earth Surf. Dyn. 6, 809–828.
Rossato, S., Mozzi, P., 2016. Inferring LGM sedimentary and climatic changes in the southern Eastern Alps foreland through the analysis of a 14C ages database (Brenta megafan, Italy). Quat. Sci. Rev. 148, 115–127.
Sacco, F., 1927. Il Glacialismo Nella Valle d'Aosta. 2 Carte 1:100.000 (Min. LL. PP., Uff. Idrog. Po, Parma).
Sacco, F., 1892. L' anfiteatro morenico del Lago Maggiore, Annali della R. Accademia d'Agricoltura di Torino.
Scapozza, C., Ambrosi, C., 2021. Between glaciers, rivers and lakes: the geomorphological landscapes of Ticino. In: Reynard, E. (Ed.), Landscapes and Landforms of Switzerland. World Geomorphological Landscapes. Springer, Cham, pp. 325–336.
Scapozza, C., Antognini, M., Oppizzi, P., Patocchi, N., 2012. Stratigrafia, morfodinamica, paleoambienti della piana fluvio-deltizia del Ticino dall'Ultimo Massimo

Glaciale a oggi: proposta di sintesi. Boll. della Soc. Ticin. di Sci. Nat. 100, 89–106.
Scapozza, C., Castelletti, C., Soma, L., Dall'Agnolo, S., Ambrosi, C., 2014. Timing of LGM and deglaciation in the southern Swiss Alps. Géomorphol. Relief, Process. Environ. 4, 307–322.
Schmidt, R., Wunsam, S., Brosch, U., Fott, J., Lami, A., Löffler, H., Marchetto, A., Müller, H.W., Praz, M., Schwaighofer, B., 1998. Late and post-glacial history of meromictic Längsee (Austria), in respect to climate change and anthropogenic impact. Aquat. Sci. 60, 56–88.
Seguinot, J., Ivy-Ochs, S., Jouvet, G., Huss, M., Funk, M., Preusser, F., 2018. Modelling last glacial cycle ice dynamics in the Alps. Cryosphere 12, 3265–3285.
Spötl, C., Koltai, G., Jarosch, A.H., Cheng, H., 2021. Increased autumn and winter precipitation during the last glacial maximum in the European Alps. Nat. Commun. 12.
Starnberger, R., Rodnight, H., Spötl, C., 2011. Chronology of the last glacial maximum in the Salzach palaeoglacier area (eastern Alps). J. Quat. Sci. 26, 502–510.
Stone, J.O., 2000. Air pressure and cosmogenic isotope production. J. Geophys. Res. Solid Earth 105, 23753–23759.
Stone, J.O., Allan, G.L., Fifield, L.K., Cresswell, R.G., 1996. Cosmogenic chlorine-36 from calcium spallation. Geochem. Cosmochim. Acta 60, 679–692.
Stone, J.O., Fifield, K., Vasconcelos, P., 2005. Terrestrial chlorine-36 production from spallation of iron. In: 10th Int. Conf. Accel. Mass Spectrom. Abstr.
Stone, J.O.H., Evans, J.M., Fifield, L.K., Allan, G.L., Cresswell, R.G., 1998. Cosmogenic chlorine-36 production in calcite by muons. Geochem. Cosmochim. Acta 62, 433–454.
Svensson, A., Andersen, K.K., Bigler, M., Clausen, H.B., Dahl-Jensen, D., Davies, S.M., Johnsen, S.J., Muscheler, R., Rasmussen, S.O., Röthlisberger, R., Peder Steffensen, J., Vinther, B.M., 2006. The Greenland Ice Core Chronology 2005, 15-42 ka. Part 2: comparison to other records. Quat. Sci. Rev. 25, 3258–3267.
Synal, H.A., Bonani, G., Döbeli, M., Ender, R.M., Gartenmann, P., Kubik, P.W., Schnabel, C., Suter, M., 1997. Status report of the PSI/ETH AMS facility. Nucl. Instruments methods phys. Res. Sect. B Beam interact. With mater. Atoms 123, 62–68.
Taramelli, T., 1870. Dell'esistenza nel versante meridionale delle alpi in relazione coi bacini lacustri e dell' origine die terrazzi allluvionali. In: Atti del Reale Istituto veneto di scienze, lettere ed arti 3, pp. 2193–2273.
Uggeri, A., Felber, M., Bini, A., Bignasca, C., Heller, F., 1997. The Valle della fornace succession. Geol. Insubrica 2, 69–80.
van Husen, D., 1997. LGM and late-glacial fluctuations in the Eastern Alps. Quat. Int. 38–39, 109–118.
van Husen, D., 1987. Das Gebiet des Traungletschers, Oberösterreich eine Typregion des Würm-Glazials. In: Mitteilungen der Kommission für Quartärforschung der Österreichischen Akademie der Wissenschaften, Bd. 7. Verlag der Österreichischen Akademie der Wissenschaften, Wien.
van Husen, D., 1977. Zur Fazies und Stratigraphie der jungpleistozänen Ablagerungen im Trauntal. Geologische Bundesanstalt, Wien.
van Husen, D., Ivy-Ochs, S., Alfimov, V., 2007. Mechanism and age of late glacial landslides in the calcaerous Alps: the Almtal, upper Austria. Austrian. J. Earth Sci. 100, 114–126.
Venzo, S., 1965. Rilevamento geologico dell'Anfiteatro morenico frontale del Garda dal Chiese all'Adige, Memorie della Società italiana di scienze naturali e del Museo civico di storia naturale di Milano. Società, Milano.
Višnjević, V., Herman, F., Prasicek, G., 2020. Climatic patterns over the European Alps during the LGM derived from inversion of the paleo-ice extent. Earth Planet Sci. Lett. 538, 116185.
Vockenhuber, C., Miltenberger, K.U., Synal, H.A., 2019. 36Cl measurements with a gas-filled magnet at 6 MV. Nucl. Instruments methods phys. Res. Sect. B Beam interact. With mater. Atoms 455, 190–194.
Winterberg, S., Picotti, V., Willett, S.D., 2020. Messinian or Pleistocene valley incision within the southern Alps. Swiss J. Geosci. 113, 7.
Wirsig, C., Zasadni, J., Christl, M., Akçar, N., Ivy-Ochs, S., 2016a. Dating the onset of LGM ice surface lowering in the High Alps. Quat. Sci. Rev. 143, 37–50.
Wirsig, C., Zasadni, J., Ivy-Ochs, S., Christl, M., Kober, F., Schlüchter, C., 2016b. A deglaciation model of the Oberhasli, Switzerland. J. Quat. Sci. 31, 46–59.
Wüthrich, L., Morabito, E.G., Zech, J., Trauerstein, M., Veit, H., Gnägi, C., Merchel, S., Scharf, A., Rugel, G., Christl, M., Zech, R., 2018. 10Be surface exposure dating of the last deglaciation in the Aare Valley, Switzerland. Swiss J. Geosci. 111, 295–303.